microLife, 2022, **3**, 1–18
DOI: 10.1093/femsml/uqac010
Advance access publication date: 29 June 2022
Research Article

Antibiotic tolerance in environmentally stressed *Bacillus subtilis*: physical barriers and induction of a viable but nonculturable state

Luiza P. Morawska and Oscar P. Kuipers*

Molecular Genetics Group, Groningen Biomolecular Sciences and Biotechnology Institute, University of Groningen, Nijenborgh 7, 9747 AG Groningen, Netherlands
***Corresponding author:** Molecular Genetics Group, Groningen Biomolecular Sciences and Biotechnology Institute, University of Groningen, Nijenborgh 7, 9747 AG Groningen, Netherlands. Tel: +31 50 36 32093, E-mail: o.p.kuipers@rug.nl
One sentence summary: Population-wide and single-cell studies on the adaptational changes of Bacillus subtilis to osmotic shifts and positive hysteresis to aminoglycoside antibiotics identified a new cell phenotype tolerant to lethal concentrations of kanamyc.

Abstract

Bacterial communities exposed to rapid changes in their habitat encounter different forms of stress. Fluctuating conditions of the microenvironment drive microorganisms to develop several stress responses to sustain growth and division, like altering gene expression and changing the cell's physiology. It is commonly known that these protection systems may give rise to differently adapted subpopulations and indirectly impact bacterial susceptibility to antimicrobials. This study focuses on the adaptation of a soil-dwelling bacterium, *Bacillus subtilis*, to sudden osmotic changes, including transient and sustained osmotic upshift. Here, we demonstrate that physiological changes caused by pre-exposure to osmotic stress facilitate *B. subtilis*' entry into a quiescent state, helping them survive when exposed to a lethal antibiotic concentration. We show that the adaptation to transient osmotic upshift with 0.6 M NaCl causes decreased metabolic rates and lowered antibiotic-mediated ROS production when cells were exposed to the aminoglycoside antibiotic kanamycin. Using a microfluidic platform combined with time-lapse microscopy, we followed the uptake of fluorescently labelled kanamycin and examined the metabolic activity of differently preadapted populations at a single-cell level. The microfluidics data revealed that under the conditions tested, *B. subtilis* escapes from the bactericidal activity of kanamycin by entering into a nongrowing dormant state. Combining single-cell studies and population-wide analysis of differently preadapted cultures, we demonstrate that kanamycin-tolerant *B. subtilis* cells are entrapped in a viable but nonculturable (VBNC) state.

Keywords: antibiotic tolerance, osmotic stress, *Bacillus subtilis*, VBNC, ROS, kanamycin

Introduction

Unlike laboratory-controlled conditions, natural microbial habitats are very dynamic and unpredictable. In nature, fluctuations of environmental conditions vary in type (e.g. suboptimal temperatures, UV radiation, shifts in osmolality and pH, nutrients availability, and presence of antimicrobial compounds) and manifest at different times and intensities. This uncertainty strongly influences the bacterial lifestyle and requires bacteria to monitor the environment, activate various stress responses, and continuously adapt their physiology to survive. However, the adaptation to many environmental stresses may result in slower growth rates and cause metabolic readaptations (Guo and Gross 2014, Soufi et al. 2015, O'Brien et al. 2016, Anand et al. 2019, Nieß et al. 2019). This fitness trade-off can be considered advantageous since reduced growth rates and entry into a low metabolic state can promote a subpopulation to enter into a so-called dormant or quiescent state in order to increase the long-term fitness of the progeny (Balaban et al. 2004, Kussell et al. 2005, Lewis 2007, Rittershaus et al. 2013, Kotte et al. 2014, Ray et al. 2016). Significantly, these highly tolerant cell variants can withstand prolonged periods of antibiotic pressure and rapidly revive upon suitable conditions; therefore, they are often related to recurring infections (Mulcahy et al. 2010, Fauvart et al. 2011, Fisher et al. 2017).

Microorganisms display several phenotypes that endure harsh environmental conditions in a viable but nonreplicating state, including persister and viable but nonculturable (VBNC) states (Ayrapetyan et al. 2018). Persisters and VBNC cells are stochastically present in the population (Ayrapetyan et al. 2015a, Manuse et al. 2021), however, they can also be generated by environmental stresses (Nowakowska and Oliver 2013, Helaine and Kugelberg 2014, Kubistova et al. 2018). These dormant cell variants can be differentiated from truly dormant endospores since, unlike spores, they maintain basal metabolic rates throughout the period of stress (Amato et al. 2013, Kotte et al. 2014, Radzikowski et al. 2016) and do not undergo evident morphological changes. Despite the metabolic capacity of persisters and VBNC cells to revive when the stressor is removed, VBNC cells have lost their ability to regrow immediately on a medium that typically supports proliferation (Oliver and Bockian 1995, Oliver 2000, Oliver et al. 2005, Nowakowska and Oliver 2013, Ayrapetyan et al. 2015a). While persisters can rapidly regrow on growth-promoting media, the VBNC cells require prolonged treatment to regain full culturability. Thus, it has been proposed that these coexisting survival strategies are part of a dormancy continuum in which persisters can progress into a deeper dormancy state and become VBNC cells (Ayrapetyan et al. 2015a, 2015b, Pu et al. 2019).

Received: May 12, 2022. **Accepted:** May 26, 2022

As a soil bacterium, *Bacillus subtilis* is exposed to frequent changes in its environment (Earl et al. 2008). For example, because of interchanging periods of flooding and drying of the upper layers of the soil, *B. subtilis* is continuously exposed to osmotic stress (Hoffmann and Bremer 2016). To survive under hypo- and hyperosmotic conditions, it employs a step-wise response strategy to maintain turgor, minimize cellular damage, and proliferate (Whatmore et al. 1990, Brill et al. 2011, Wood 2011, Hoffmann and Bremer 2016, Bremer and Krämer 2019). Notably, the cellular adaptations to the osmotic stress result in a reduced growth rate, contributing to increased antibiotic tolerance. This is primarily because of the immediate changes in turgor pressure and membrane tension, which directly modify the elongation rates by inhibiting peptidoglycan synthesis (Misra et al. 2013, Rojas et al. 2017, Rojas and Huang 2018). Second, the adaptation to the osmotic stress comes with an energetic cost due to the activation of the general stress response and the metabolic rerouting towards a so-called osmo-adaptive pathway to synthesize and maintain a pool of osmoprotectants. These metabolic adaptations can interfere with other metabolic processes by allocating carbon resources and energy to the synthesis of an osmo-specific proteome instead of into anabolic pathways (Hahne et al. 2010, Schroeter et al. 2013, Kohlstedt et al. 2014, Sévin and Sauer 2014, Sévin et al. 2016, Nieß et al. 2019, Godard et al. 2020).

High salt environments are also present in the human body, hence, it is essential to determine the mechanisms used by microorganisms to differentiate under these conditions and become resistant to antibiotics. Here, we examined the adaptation of *B. subtilis* to osmotic stress and studied its resilience to aminoglycoside antibiotics upon osmotic upshifts. We observed that growth behavior and physiology in presence of aminoglycosides differed depending on the prior preadaptation with osmotic stress. Furthermore, we studied single cell morphological and physiological changes in microfluidics in response to fluorescently labelled kanamycin and osmotic adaptation. This study shows how osmotic shifts modulate *B. subtilis* membrane potential and metabolic activity and promote the entry into the VBNC state when treated with lethal doses of kanamycin.

Methods

Bacterial strains, culture conditions, and media

All tested strains used in this study are derivatives of the *B. subtilis* 168 *trpC2* laboratory strain. *Bacillus subtilis* strains were grown in Spizizen's Minimal Medium (Harwood and Cutting 1990; 1XSMM) supplemented with 0.5% (w/v) glucose, 1% (v/v) trace elements and, for tryptophan-autotroph strains, 0.5% (w/v) tryptophan. To maintain the same culture conditions, the 3-day cultivation was performed as follows: *B. subtilis* was streaked on selective LB agar plates and incubated overnight (O/N) at 37°C. The next morning, 3 ml liquid LB was inoculated with a single colony and incubated for 8 hours at 37°C and 220 rpm. After the incubation period, the culture was diluted 1:1000 in supplemented 1XSMM medium and grown O/N at 37°C and 220 rpm. The overnight culture was diluted to OD600 of 0.08 in fresh 1XSMM medium and grown until the OD600 reached a value of 0.3. The exponentially growing culture was immediately subjected to osmotic stress, and the following measurements described below were taken when appropriate.

Antibiotic resistance screening

Antibiotic resistance was tested in 96-well microtiter plates using a Varioskan™ LUX multimode microplate reader (Thermofisher). An exponentially growing culture was grown in complete SMM with or without 0.6 M NaCl for 90 minutes and centrifuged at 4000 relative centrifugal force (rcf) for 3 minutes. The cell pellet was resuspended in fresh SMM with (sustained osmotic upshift) or without 0.6 M NaCl (sudden osmotic downshift) to the final OD600 of 0.1. Subsequently, cells were loaded into a 96-well microtiter plate containing a series of dilutions of tested antibiotics. The final volume of culture was 135 μl per well. OD600 measurements were performed at 37°C and 220 rpm, every 5 minutes over 18 hours. At least two independent experiments were performed for each condition.

Microfluidics experiments

The experiments were performed with the CellASIC ONIX microfluidic device (Merck Millipore) in a B04A plate. The plate was primed with the medium before the experiment, using the manufacturer's specifications. A pump pressure of 0.25 psi drove the flow rate of the supplied medium. Exponentially growing cells were diluted in the complete SMM to OD600 0.05 and subsequently loaded on the microfluidics plate. The microfluidic plate was mounted on an Olympus IX71 DeltaVision microscope, for fluorescence time-lapse microscopy. The changes of growth conditions in each chamber were performed accordingly: preadaptation with or without 0.6 M NaCl SMM; antibiotic treatment with 62.5 μg/ml kanamycin in SMM with (sustained osmotic upshift) or without 0.6 M NaCl (sudden osmotic downshift); of SMM. The exposure time to each condition is indicated in the manuscript accordingly. Cells were tracked by imaging phase-contrast and fluorescence every 15 minutes, typically over 24 hours. All experiments were performed at 37°C.

Single-cell analysis of growth rates and the fluorescent signal from time-lapse microscopy

Single-cell tracking and data analysis were performed with ImageJ software and MicrobeJ plugin (Ducret et al. 2016). The relative growth of the cell was determined from the cell volumes (μm^3), determined with: $V = 0.549 \cdot A^{2/3}$ (Zeder et al. 2011), at successive time points. Once a growing population has reached a steady-state, the calculation of growth rates was performed in GraphPad Prism 8, by fitting data into the Malthusian exponential growth equation.

Kanamycin uptake measurements

Kanamycin uptake was measured with a conjugate of kanamycin–Texas Red. The conjugate was synthesized with Texas Red™-X, the Succinimidyl Ester Labeling kit (Thermofisher) according to the manufacturer's specifications: 10 mg/ml kanamycin was dissolved in 0.1–0.2 M sodium bicarbonate buffer, pH 8.3 mixed with 2 mg/ml Texas Red™-X, Succinimidyl Ester in N, N-dimethylformamide and agitated at 4°C for 72 hours. For the time-lapse experiments: to capture phase contrast and the fluorescent signal from kanamycin–Texas Red conjugate, a 60X phase contrast objective (NA 1.4, oil-immersion, DV) was used. The mCherry filter set with exposure time 0.5 seconds and transmission 10% was used to visualize the conjugate.

Reactive oxygen species measurements

Reactive oxygen species (ROS) levels were measured using 10 μM of 2',7'-dichlorofluorescein diacetate (H_2DCFDA) fluorescent dye. All measurements were performed in 96-well black microtiter plates using Varioskan™ LUX multimode microplate reader (Thermofisher). An exponentially growing culture was exposed to 0.6 M

NaCl for 90 minutes, diluted to an OD600 of 0.1 in fresh SMM with or without 0.6 M NaCl, and exposed to antibiotics. Final microtiter plate volume was 135 μl per well. OD600 was measured every 5 minutes over 18 hours. At least two independent experiments were performed for each condition. Fluorescence was measured with excitation at 488 nm and emission at 510 nm. The control without H_2DCFDA was used to correct for autofluorescence.

Membrane potential measurements

An exponentially growing culture was exposed to SMM with or without 0.6 M NaCl for 90 minutes, diluted to an OD600 of 0.08 in fresh SMM with or without 0.6 M NaCl and exposed to antibiotics. Membrane potential dynamics were measured using Thioflavin-T (ThT)—a cationic Nernstian dye, at 10 μM. ThT fluorescence is known to increase when the inside of the cell becomes more negative; therefore, ThT is inversely related to the membrane potential. For the time-lapse microscopy and 96-well plates experiments, the excitation: 440 nm and emission: 490 nm was used to measure the fluorescence. In the case of microtiter plate experiments, for the positive control, 5 μM of carbonyl cyanide m-chlorophenyl hydrazone (CCCP) was added to the nonstressed culture to quench the membrane potential.

Intracellular ATP levels

ATP levels of antibiotic-treated cells were determined with the BacTiter-Glo™ microbial cell viability assay kit (Promega). A total of 5 μM of CCCP was used as a positive control. Measurements were performed every hour for a total time of 4 hours postantibiotic treatment. At each time point, 100 μl cell culture was added to 100 μl BacTiter-Glo™ reagent and incubated at room temperature for 5 minutes. Luminescence was measured with a Tecan Infinite F200 Pro luminometer. The intracellular ATP concentration was determined with a standard curve made with a commercial ATP solution.

VNBC cell estimation

The fraction of VNBC cells of sporulation-deficient *B. subtilis* 168 Δ*sigF* after 18 hours of 62.5 μg/ml kanamycin treatment was estimated using, a CytoFLEX S Flow Cytometer (Beckman Coulter) and the LIVE/DEAD™ BacLight™ Bacterial Viability Kit (ThermoFisher) with the green-fluorescent SYTO 9 dye and red-fluorescent propidium iodide (PI). SYTO 9 labels all bacteria in a population—those with intact membranes and those with damaged membranes. In contrast, PI preferentially penetrates bacteria with damaged membranes, causing a reduction in the SYTO 9 stain fluorescence when both dyes are present. Therefore, decreased green fluorescence and increased red fluorescence indicate a damaged population. Before the measurements, samples were stained accordingly to the manufacturer's suggestions, and diluted 2-fold in phosphate-buffered saline buffer [PBS, Boom (Oxoid)]. Subsequently, 100 000 events were recorded and the data was analyzed in the FlowJo 7 software.

Results

Environmentally stressed *B. subtilis* is more tolerant to kanamycin

To investigate the effects of osmotic stress on antibiotic tolerance development, we designed a step-wise adaptation experiment in which we emulated sudden environmental shifts and followed the outgrowth of the well-characterized laboratory strain *B. subtilis* 168 (Fig. 1). Liquid cultures of *B. subtilis* 168 were preadapted to

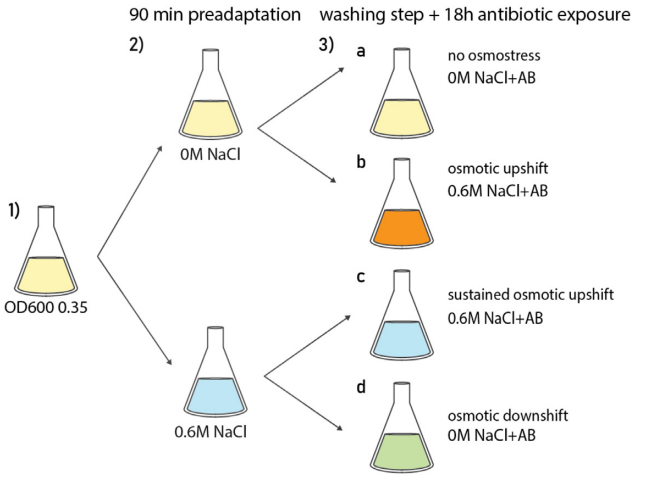

Figure 1. Schematic representation of the experimental setup. The exponentially growing culture of *B. subtilis* 168 in SMM was divided into two equal parts. (1) One part of the culture was exposed to 0.6 M NaCl for 90 minutes, whereas the control (the yellow flask) continued to grow in SMM media without salt. (2) After 90 minutes, cells from all the samples were collected and washed with appropriate fresh media and their OD600 was adjusted to 0.1. Nonstressed cells were washed with fresh SMM without (3a) and with 0.6 M NaCl (3b), resulting in nonstressed control cells and cells exposed to osmotic upshift. Preadapted with salt, cells were washed with fresh SMM with (3c) or without (3d) 0.6 M NaCl, resulting in cells growing in sustained hyperosmotic conditions and experiencing transient hypo-osmotic stress, respectively. All cultures were subsequently exposed to increasing concentrations of kanamycin, and the outgrowth was monitored for 18 hours.

a nonlethal concentration of sodium chloride (0.6 M NaCl) for 90 minutes to activate the general stress response and synthesize a sufficient amount of proline to protect the cell from adverse effects of water outflow and prolonged plasmolysis (Brill et al. 2011; Fig. 1.2). After the preadaptation step, the osmotically challenged cells were transferred to fresh media with or without salt, and their susceptibility to aminoglycosides was tested (Fig. 1.3). Subsequently, we performed dose-response assays with increasing antibiotic concentrations and followed the growth of all the bacterial populations (Fig. 2). All experiments were conducted in SMM minimal media supplemented with 0.5% glucose as a primary carbon source to avoid severe starvation conditions and limit sporulation.

The analysis of the outgrowth data showed that *B. subtilis* responds to 90 minutes of hyperosmotic stress with suppressed growth, observed by a substantial decrease in growth rate (μ; Fig. 2A). This reduced growth may result directly from mechanical stress of the cell envelope (Misra et al. 2013, Rojas et al. 2017), as well as from metabolic shifts towards activating general stress response and synthesizing osmoprotectants induced under prolonged osmotic upshift (Kohlstedt et al. 2014, Godard et al. 2020).

Comparing the growth-inhibition profiles of differently preadapted cultures exposed to kanamycin revealed that cells continuously exposed to 0.6 M NaCl could grow and divide at all kanamycin concentrations tested and survive even 16 times the minimal inhibitory concentration (15.625 μg/ml; Fig. 2B and C). In this particular case, for almost all concentrations tested, the growth behavior was unaffected by the presence of kanamycin, resembling the outgrowth of cells without antibiotics. Similar growth behavior was observed for cells exposed simultaneously to 0.6 M NaCl and kanamycin (Fig. 2D), showing that the 90 minutes preadaptation period is not essential for cells to become kanamycin-insensitive when continuously growing in the pres-

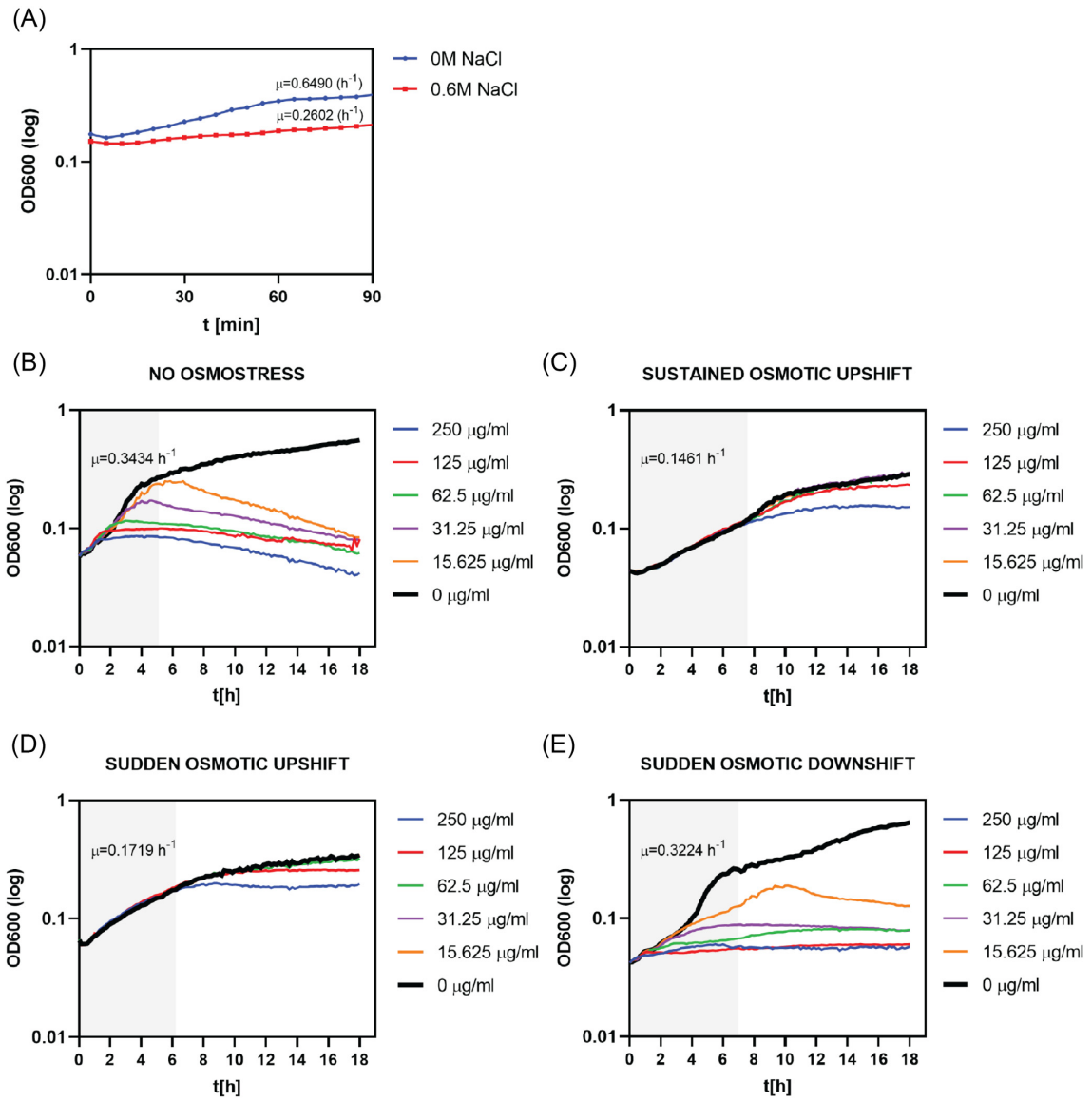

Figure 2. Aminoglycoside tolerance of osmotically preadapted culture of *B. subtilis* 168. Growth curves for *B. subtilis* 168 during and after 90 minutes of 0.6 M NaCl pretreatment in SMM. **(A)** Represents the outgrowth of cultures during the pretreatment step with indicated growth rate values in h^{-1} (μ). **(B)–(E)** Represent the outgrowth of differently preadapted *B. subtilis* cultures in the presence of increasing concentrations of kanamycin (0–250 μg/ml). (B) Shows the control conditions without osmostress pretreatment. The black curve indicates the outgrowth of cultures without antibiotics for each experiment. The shaded area of growth was taken into calculations of growth rates of the control samples without kanamycin, with μ indicating values (h^{-1}). The calculations of doubling time were determined in GraphPad Prism 8 using nonlinear regression fit analysis (Malthusian exponential growth) based on the period of exponential growth marked with shaded areas. All measurements were performed in biological triplicates, and the mean values were plotted on the graphs. Error bars (SEM, $n = 3$)

ence of sodium chloride. Following these observations, we tested a range of different classes of antibiotics (Table 1) to determine whether the sensitivity of *B. subtilis* to tested antibiotics changed when cells were growing in a sustained osmotic upshift. Amongst all tested antibiotics, the outgrowth experiments showed that the most prominent protective effect was present only when cells were exposed to bactericidal aminoglycosides: kanamycin and gentamycin (Figure S1, Supporting Information). This indicates that despite reduced growth rates (Fig. 2C), the susceptibly of osmotically stressed cells to other antibiotics was not significantly affected.

Interestingly, in the case of sudden osmotic downshift, we found that the cells were not as insensitive to kanamycin as those exposed to prolonged osmotic upshift, but also not entirely susceptible as the untreated cells (no osmostress; Fig. 2E). Additionally, after 5 hours of drug exposure, we did not observe a decrease in optical density, characteristic of cells without a pretreatment step. Instead, the OD600 values indicated that cells experiencing simultaneous osmotic downshift and kanamycin treatment do not lyse.

Changes in the membrane potential indicate limited kanamycin uptake in osmostressed *B. subtilis*

Aminoglycosides are broad-spectrum antibiotics commonly used to control Gram-negative and some Gram-positive bacterial infections. Their bactericidal effect has been long studied; however, their exact mechanisms of action are still- and long-discussed (Kohanski et al. 2007, 2010, Ezraty et al. 2013, Keren et al. 2013, Bruni and Kralj 2020, Damper and Epstein 1981). To date, it is

Table 1. Summary of the cross-protection experiments with different classes of antibiotics. *Bacillus subtilis* 168 was preadapted with 0.6 M NaCl and tested against different classes of antibiotics with different targets and mechanisms of action.

Antibiotic	Class	Target	Bactericidal/bacteriostatic	Protection in sustained osmotic upshift
Kanamycin	**Aminoglycosides**	**30 s ribosome subunit**	**Bactericidal**	**Yes**
Gentamicin	**Aminoglycosides**	**30 s ribosome subunit**	**Bactericidal**	**Yes**
Ehromycin	Macrolides	50 s ribosome subunit	Bacteriostatic	No
Ciprofloxacin	Fluoroquinolones	DNA gyrase	Bactericidal	No
Spectinomycin	Aminocyclitols	30 s ribosome subunit	Bacteriostatic	No
Tetracycline	Polyketides	30 s ribosome subunit	Bacteriostatic	No

known that aminoglycosides impair protein synthesis by binding to the 70S ribosome (Borovinskaya et al. 2007, Taber et al. 1987). The misfolded proteins cause several adverse secondary effects that lead to cell death, including membrane damage, positive feedback of drug uptake, and the formation of highly toxic ROS (Hancock et al. 1981, Nichols and Young 1985, Davis et al. 1986, Kohanski et al. 2007, 2010, Ramirez and Tolmasky 2010, Ezraty et al. 2013, Taber et al. 1987). However, aminoglycosides need to be transported inside the bacterial cell to reach bacterial ribosomes. Previous studies showed that the uptake of aminoglycosides is an energy-dependent process and is intrinsically tied to membrane potential (Leviton et al. 1995, Damper and Epstein 1981, Taber et al. 1987), yet the recent work of Bruni and Kralj (2020), elegantly showed that aminoglycosides could be transported inside the cell with dissipated membrane potential. Nevertheless, the high membrane potential facilitates the uptake of aminoglycosides, and since exposure to osmotic stress can induce changes in respiration and reduce the membrane potential, we reasoned that osmotically challenged *B. subtilis* cells limited the uptake of aminoglycosides (Fig. 2D).

To investigate the changes in membrane potential of differently pretreated populations, we followed the fluorescent signal changes from ThT, a cationic Nernstian dye. Because ThT binds to hyperpolarized membranes (negatively charged), the measured fluorescent signal inversely correlates with the membrane potential (Prindle et al. 2015, Humphries et al. 2017). Microscopic analysis of the ThT fluorescence revealed that membranes of osmotically challenged cells were less negatively charged than the membranes of untreated cells, indicating a decreased membrane potential after 90 minutes of salt pretreatment (Fig. 3A). Additionally, the outgrowth experiments showed that exposure of untreated cells to kanamycin induces membrane polarization and increases the membrane potential upon the antibiotic's entry (Fig. 3B). The following correlation was found: the higher the antibiotic concentration, the higher the polarization of the membranes. Moreover, kanamycin caused prolonged membrane hyperpolarization. This data supports the proposed killing mechanism of bactericidal antibiotics targeting translation, including aminoglycosides, which display membrane hyperpolarization directly preceding cell lysis (Kohanski et al. 2007, Lobritz et al. 2015, Lee et al. 2019, Bruni and Kralj 2020). The level of hyperpolarization depends on the amount of antibiotic that can penetrate the cell envelope, impair translation, cause protein mistranslation, and induce membrane pore formation.

Interestingly, a similar correlation between membrane hyperpolarization and antibiotic concentration was found with a sudden osmotic downshift treatment (Fig. 3C). However, here the induced membrane hyperpolarization due to the antibiotic treatment did not cause cell lysis. The differences in the ThT signal intensity between cells with and without the 90 minutes of salt pretreatment may result from the changes in the membrane potential upon osmotic shifts (Fig. 3A).

For the cells exposed to sustained osmotic stress, kanamycin treatment did not cause severe membrane hyperpolarization (Fig. 3D), as observed for kanamycin-sensitive cells. Moreover, the antibiotic concentration-dependent effect on membrane polarization was less prominent, suggesting that the presence of 0.6 M NaCl in the media reduced the uptake of kanamycin. Interestingly, the cells exposed to the highest kanamycin concentrations displayed severely reduced growth, indicating that a sufficient amount of the administered kanamycin could enter the cell and reduce its growth rate; however, it did not cause membrane hyperpolarization (Fig. 3D). Both the outgrowth and ThT measurements indicate that for the highest antibiotic concentration, the 0.6 M NaCl treatment averted the bactericidal effects of kanamycin by likely reducing its intracellular levels. Taken all together, we propose that under sustained osmotic stress conditions, the entry of kanamycin is limited, enabling *B. subtilis* cells to tolerate the killing concentrations of kanamycin in the media.

ROS formation in antibiotic-treated cultures reflects the kanamycin-induced cell damage in environmentally stressed *B. subtilis*

It has been proposed that aminoglycosides, upon entry, impose cell damage by impeding protein translation and inducing envelope stress response (Davis et al. 1986, Busse et al. 1992, Kohanski et al. 2008). However, when the primary damage is insufficient in killing the cells, the downstream cascade of events induces secondary damage by accumulating lethal concentrations of ROS (Hong et al. 2019). Therefore, to investigate the lethal effect of kanamycin on *B. subtilis* cells, we followed the ROS formation in bulk cultures. To follow the changes in the ROS pools of the antibiotic-treated cultures, we used 2',7'-dichlorodihydrofluorescein diacetate (H_2DCFDA), a chemically reduced form of fluorescein. Inside the cell, H_2DCFDA is cleaved by intracellular esterases and oxidized in the presence of hydroxyl radicals to the highly fluorescent 2',7'-dichlorofluorescein (DCF). Thus, the conversion of H_2DCFDA to DCF directly corresponds to the ROS levels.

Unsurprisingly, for the control cells without the pretreatment step, the analysis of changes in fluorescent signal indicated a significant increase in ROS formation upon antibiotic treatment (Fig. 4A). The most severe increase in the fluorescent signal was observed after 5 hours and highly correlated with increased cell lysis, showing that ROS accumulation results from

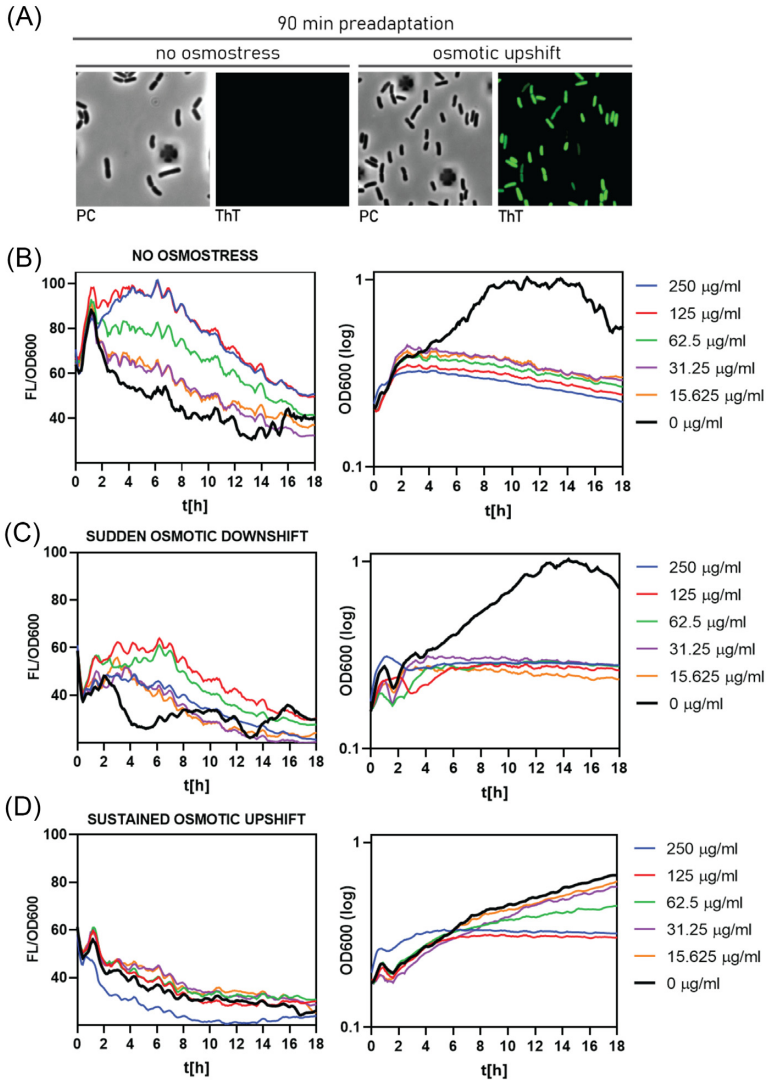

Figure 3. Membrane potential measurements in differently adapted *B. subtilis* 168 cultures. **(A)** Micrographs of *B. subtilis* grown in SMM with and without 0.6 M NaCl for 90 minutes prior to antibiotic exposure. For the outgrowth measurements experiment, **(B)–(D)** differently pretreated cultures of *B. subtilis* 168 were washed and transferred to a 96-well plate with fresh media with or without 0.6 M NaCl in the presence of kanamycin and ThT and diluted to the starting OD600 = 0.2. The left side panels represent measurements of relative fluorescent signal of ThT from (B)—untreated cells, (C)—cells experiencing sudden osmotic downshift, and (D)—cells exposed to sustained osmotic upshift. Panels on the right show the outgrowth data of differently preadapted cultures, respectively. The black curve indicates the outgrowth of cultures without antibiotics for each experiment. Graphs show the mean signal from two independent biological replicates.

induced cell death by kanamycin. Interestingly, up to 125 µg/ml kanamycin concentration, we observed a dose-dependent effect of kanamycin on ROS accumulation in kanamycin-sensitive cells (Fig. 4A and D).

In the case of cells that underwent sudden osmotic downshift (Fig. 4B), the intracellular ROS levels were significantly lower than the kanamycin-sensitive cells. At 5 hours postantibiotic treatment, the intensity of DCF fluorescence was 3.6-fold lower than that of kanamycin-sensitive cells, at 125 µg/ml kanamycin. A similar effect was observed for the cells exposed to the sustained osmotic upshift (3.8-fold change; Fig. 4D). Cumulatively, hydroxyl radical results suggest that in the case of the sudden osmotic downshift, the bactericidal effects of kanamycin are less severe than that of kanamycin-sensitive cells. Although the pretreated cells accumulate kanamycin, their biochemical response to the antibiotic is less severe than that of untreated cells.

Kanamycin uptake at the single-cell level

To better understand the physiology of antibiotic-resistant cells and complete the study on the antibiotic uptake at the single-cell level, we performed time-lapse microscopy with a fluorescently labelled kanamycin-Texas Red conjugate. Using microfluidics, we applied various conditions sequentially and followed the cells' response to the sudden environmental changes. Accordingly, we exposed exponentially growing cultures of *B. subtilis* to the following conditions: 90 minutes of preadaptation to osmotic upshift, 16 hours of kanamycin-Texas Red exposure, and 5 hours of optimal growth conditions in SMM (Fig. 5A–C). Additionally, since the switch between different osmolarity environments is very rapid (i.e. sudden osmotic downshift) and cells have limited time to recover from the pretreatment conditions, we tested whether a longer readaptation to neutral osmolarity could boost the growth rates and consequently increase the sensitivity to kanamycin (Fig. 5D).

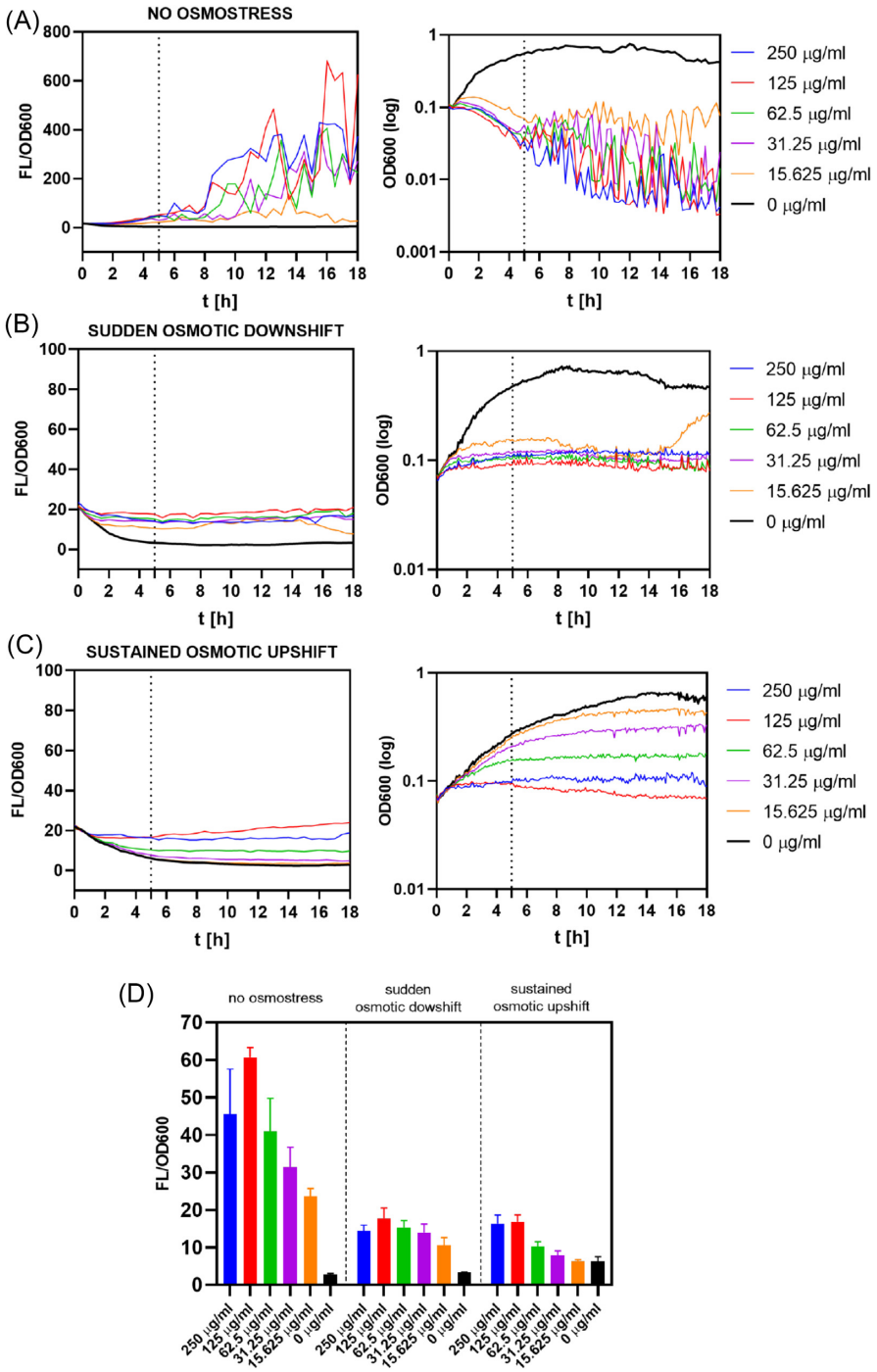

Figure 4. Measurement of ROS levels in kanamycin-treated *B. subtilis* 168 cultures with and without 0.6 M NaCl pretreatment. The exponentially growing *B. subtilis* 168 cells were first exposed to 0.6 M NaCl for 90 minutes in a growing culture in a liquid medium. After the pretreatment step, cells were supplemented with H_2DCFDA and subsequently transferred to a 96-well plate with SMM media in the presence of a kanamycin gradient, and the optical density of the culture and the fluorescence were measured using the microplate reader for 18 hours. Graphs represent measurements of relative fluorescent signal of DCF from **(A)**—untreated cells, **(B)**—cells exposed to sustained osmotic stress, and **(C)**—cells experiencing sudden osmotic downshift. The black curve indicates the outgrowth of cultures without antibiotics for each experiment. Graphs show the mean signal from three independent replicates. The black dotted line indicates 5 hours of antibiotic treatment. **(D)**—Shows the comparison of DCF fluorescence at 5 hours' time point across tested conditions.

The single-cell analysis confirmed previous observations of distinct growth behaviors for differently preadapted *B. subtilis* cultures (Figure S2, Supporting Information). Bacteria that suffered solely from antibiotic exposure (no osmostress pretreatment) displayed characteristic growth inhibition and autolysis when challenged with kanamycin (Fig. 6A). We observed that the autolysis was preceded by cytoplasmic condensation and a protein aggregation phenotype, typical of aminoglycoside treatment, manifested with dark bodies at the cell poles and phase-light areas in between (Fig. 6E). After 5 hours of antibiotic exposure, the fluorescent signal from kanamycin-Texas Red was mainly localized at the cell poles and near the division sites, indicating putative entry regions

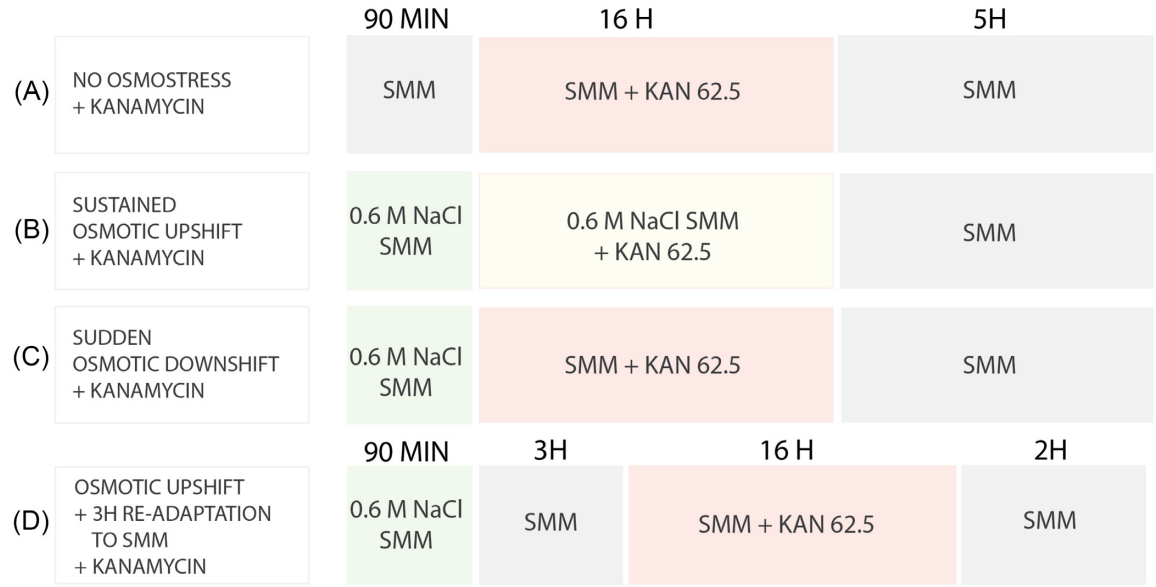

Figure 5. Schematic overview of the experimental microfluidics setup Exponentially growing cells were loaded on a commercial microfluidic plate and subjected to a series of changes in environmental conditions. Different stress conditions are depicted with different coloured boxes. Treatment time is indicated above the boxes. The final concentration of kanamycin used for the time-lapse experiments was 62.5 μg/ml.

(Fig. 6F). Further on, the conjugate gradually accumulated in the cytoplasm of the treated cells, which later displayed lysis within 16 hours of incubation (Fig. 6A). Notably, 16 hours of exposure to 62.5 μg/ml kanamycin showed high cell-to-cell variability in terms of survival. After 16 hours of incubation with antibiotics, not all the cells displayed lysis, even though the drug was accumulated inside the cell.

In the case of the sustained osmotic upshift, microscopic data revealed that kanamycin could not enter the cell (Fig. 6B and G), which explains why *B. subtilis* cells could grow and divide in the presence of kanamycin (Figure S2B, Supporting Information). The fluorescent signal from kanamycin-Texas Red™ was hardly detected and mainly localized at the cell poles and the division sites. Consequently, we did not observe any morphological changes pointing to protein aggregation and lysis. Interestingly, the intensity of the signal increased immediately when the ionic strength of the environment changed after switching to SMM (Fig. 6H and I). This boosted adsorption of the antibiotic conjugate to the cell surface after salt removal suggests that the ionic interactions between *B. subtilis*' cell surface and polycationic kanamycin are crucial for efficient drug uptake, supporting findings of Kadurugamuwa et al. (1993a,b).

In agreement with the membrane potential data, time-lapse microscopy showed that cells experiencing sudden osmotic downshift efficiently accumulated kanamycin–Texas Red (Fig. 6C and G), similarly to the untreated cells (Fig. 6A and G). After 16 hours of antibiotic treatment, all cells accumulated fluorescent conjugate; however, we did not observe protein aggregation and cell lysis, unlike in the case of untreated cells. This antibiotic-tolerant phenotype could not be revived with 5 hours of growth in drug-free SMM (Fig. 6C). Additionally, although kanamycin was removed from the environment, the previously accumulated drug was still present inside the cytoplasm, likely impairing translation and altering cell growth and division. Over time, the fluorescent signal from the conjugate decreased (Fig. 6G), suggesting that cells were able to remove or neutralize it gradually. However, cells could still not recover and form microcolonies.

Aminoglycosides are ineffective when used against slow-growing or dormant bacteria, and bacterial-resistant populations can be efficiently eradicated with metabolic stimulation by nutrients supplementation (Allison et al. 2011, Helaine and Kugelberg 2014). Since 90 minutes of osmotic upshift decreases the growth rate and membrane potential of *B. subtilis* cells, we wondered if the metabolic boost before the antibiotic treatment can resensitize pretreated cells to kanamycin. In order to boost the metabolism of slow-growing pretreated cells, we washed them with fresh media and incubated for 3 hours prior to antibiotic exposure. Interestingly, we found 3 hours of incubation in SMM resensitized cells to kanamycin (Fig. 6D). Time-lapse microscopy showed that within 3 hours, cells resumed growth and underwent two division cycles, pointing to increased metabolic rates and active protein synthesis (Figure S2D, Supporting Information). Similarly to the control conditions, readapted cells accumulated fluorescent conjugate and displayed characteristic phenotype with cytoplasmic condensation and protein aggregation (Fig. 6D). Eventually, most of the population lysed within 16 hours of antibiotic treatment.

Together, these results reveal that besides the ionic interaction between the antibiotic and the cell envelope, the differences in metabolic and proliferation rates have a detrimental effect on the survival of environmentally stressed *B. subtilis* when exposed to the bactericidal antibiotic like kanamycin. We show that extremely slow-growing cells (Figure S2C, Supporting Information) are more tolerant to critical doses of antibiotics than the fast-growing ones (Figure S2A and S2D, Supporting Information). Therefore, we speculate that metabolic adaptations due to the osmostress pretreatment and simultaneous kanamycin stress avert the bactericidal effects of kanamycin, manifested by the increased tolerance of *B. subtilis* to the antibiotic.

Pre-exposure to hyperosmotic stress promotes *B. subtilis* entry into a low-metabolic state

Entry into dormancy enables bacteria to persist for long periods under adverse conditions, including exposure to antibiotics. As the foregoing data suggest, the preadaptation to the hyperos-

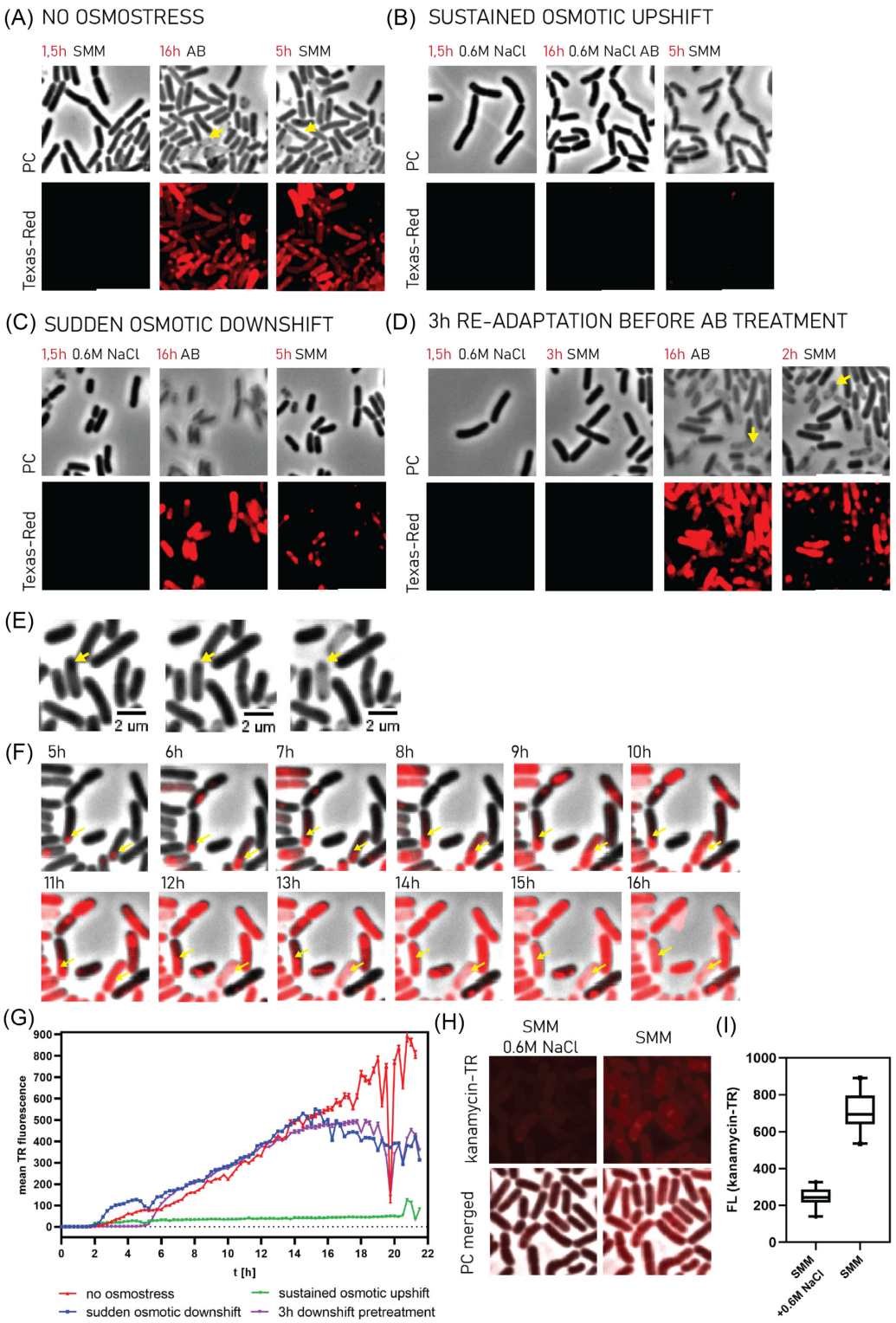

Figure 6. Uptake of fluorescently labelled kanamycin in differently preadapted *B. subtilis* 168 cultures. After reaching an OD600 of 0.35, *B. subtilis* 168 culture was transferred to the microfluidic device. Tested media were sequentially delivered to four microfluidics chambers, and time-lapse microscopy was performed. Micrographs **(A)**, **(B)**, and **(C)** show adaptation to three stages of the experiment: (1) 90 minutes of preadaptation conditions with or without 0.6 M NaCl, (2) 16 hours of kanamycin-Texas Red (72 μg/ml) exposure with or without salt, (3) 5 hours wash-out with salt- and kanamycin-free media. The last section of micrographs **(D)** includes an additional 3 hours of readaptation to SMM right before the antibiotic treatment. The upper panel of all sections shows phase contrast images, while the lower one shows the kanamycin-Texas Red conjugate signal. Yellow arrows indicate lysed cells with dark foci of protein aggregates. **(E)** Shows micrographs of antibiotic-stressed cells displaying cytoplasmic condensation and protein aggregation phenotype, indicated with yellow arrows. **(F)** Kanamycin-Texas Red uptake in untreated with salt cells after 5 hours from antibiotic administration. Cells with the fluorescent foci showing the entry of kanamycin-Texas Red (72 μg/ml) are indicated with yellow arrows. **(G)** Quantitative measurements of kanamycin-Texas Red uptake in time for all tested conditions. Single-cell measurements acquired the mean fluorescent signal from time-lapse microscopy. (H) Adsorption of kanamycin-Texas Red to *B. subtilis*' membranes after salt removal. The upper panel shows the fluorescent signal from kanamycin-Texas Red. (H) The average fluorescent signal of kanamycin-Texas Red in the presence and absence of 0.6 M NaCl in the media.

motic stress caused a significant decrease in metabolic activity and reduced growth rates. Therefore, we suspected that the population of pretreated *B. subtilis* enters dormancy and increases their tolerance to kanamycin. To provide more insights into the metabolic activity involved in developing the antibiotic-tolerant phenotype, we performed a time-lapse microscopy experiment, in which we followed metabolic changes of single cells using calcein acetoxymethyl ester (CAM). CAM conversion to calcein violet (CV) was successfully applied to distinguish nonviable cells from metabolically active but not growing cells (Krämer et al. 2015, Hendon-Dunn et al. 2016). Since only metabolically active cells can enzymatically convert nonfluorescent CAM to fluorescent CV and transport the fluorochrome out in an energy-dependent manner, the mean CV fluorescence signal obtained from a single nondividing cell, while CAM is continuously perfused with the media, offers a relative measure of its metabolic rates in time (Krämer et al. 2015). Highly energized, fast-growing cells are expected to display moderate levels of the mean CV signal due to the constant turnover of CAM. For the nongrowing but metabolically active cells, CAM conversion to CV is maintained by the intracellular esterases; however, the active export of CV is less efficient; therefore, the mean CV signal should be significantly higher than that of fast-growing cells.

Using a microfluidic system, we followed the changes in CV fluorescence across the following conditions: 90 minutes with or without 0.6 M NaCl pretreatment, 16 hours of kanamycin exposure in SMM and 5 hours of wash-out with kanamycin-free growth media. Additionally, to distinguish metabolically active nongrowing cells from dead cells, we used PI. This cationic dye preferentially penetrates cells with damaged membranes, indicating membrane discontinuity and cell lysis.

Time-lapse microscopy confirmed that the preadaptation to osmotic upshift impairs the metabolism of *B. subtilis* cells. Within 90 minutes of the preadaptation period, viable cells displayed moderate CV fluorescence, whereas the preadapted with 0.6 M NaCl cells with reduced growth rates were highly fluorescent (Fig. 7A–D). The initial differences in the CV fluorescence between actively growing cells (untreated) versus slow growing ones (pretreated) are caused by different capacity of CAM turnover. After the preadaptation period, we followed the effect of kanamycin on each culture's growth and metabolic activity. Interestingly, for both studied populations, *B. subtilis* displayed high cell-to-cell variation in the mean CV fluorescence when exposed to kanamycin (Fig. 8A and B), which can be explained by the kanamycin's interaction with the cell envelope and further membrane pore formation. Moreover, we found that in the case of untreated cells, a transient increase in the CV fluorescent signal was mainly preceding cell lysis (Fig. 7E).

For the cells exposed to sudden osmotic downshift, we observed an initial drop in the mean CV fluorescence signal after the pretreatment with 0.6 M NaCl (Fig. 7B and D); however, this change was observed due to the sudden changes in the environment's osmolarity rather than to the immediate boost in the metabolic activity. Interestingly, 3.5 hours after kanamycin administration to the media, most of the population slowly regained the CV signal, suggesting that nondividing cells gradually converted CAM, evidencing active metabolism of nondividing cells upon antibiotic treatment.

The final treatment with a drug-free medium showed that, in both studied cases, nondividing cells boosted their metabolism, indicated by the increase in the CV fluorescence on a single-cell level (Fig. 8). The metabolic boost caused a significant increase in cell death for the untreated cell, whereas, for the pretreated cells, approximately 50% of the population indicated cell damage, but we did not observe cell lysis (Figs 7F and 8B).

Kanamycin treatment upon sudden change in osmotic pressure extends membrane hyperpolarization in *B. subtilis*

The time-lapse microscopy revealed that pretreated cells after sudden osmotic downshift and exposure to a high kanamycin concentration are fixed in a nondividing but metabolically active state (Fig. 8B). Recent studies on ribosome targeting antibiotics, including kanamycin, showed that growth-defective *B. subtilis* cells exhibit a transient membrane hyperpolarization, followed by cell death (Lee et al. 2019). Importantly, it was observed that cells displayed a high cell-to-cell variation in terms of the level of membrane hyperpolarization. Previously we showed that exposure to the same concentrations of kanamycin in pretreated and untreated cells resulted in significant differences in membrane hyperpolarization on a population-wide level, indicating that pretreated cells were less affected by kanamycin (Fig. 3B and C). However, we wondered how these cells respond to kanamycin insults on a single-cell level during and postantibiotic treatment. Therefore, we evaluated the changes in membrane potential of nondividing but metabolically active cells during 10 hours of kanamycin treatment and 20 hours of readaptation to SMM on a single-cell level.

The microscopy data confirmed a significant increase in membrane hyperpolarization upon sudden osmotic downshift and kanamycin treatment (Fig. 9). The mean ThT fluorescent signal immediately increased upon osmotic downshift and antibiotic treatment and remained relatively high after the antibiotic removal (Fig. 9A). Importantly, all the cells pre-exposed to the osmotic upshift displayed similar levels of ThT fluorescence. In contrast, kanamycin-sensitive cells (no osmostressed) showed high cell-to-cell variation of membrane potential, represented by the variation in the mean ThT signal (Fig. 9A). Notably, after the first media change, for the pretreated cells the ThT signal linearly decayed in time, showing that nondividing but metabolically active cells can gradually recover membrane potential homeostasis. However, 20 hours of growth in antibiotic-free media was not sufficient to fully recover membrane potential and resume division, likely due to the remaining kanamycin (Fig. 9B).

Interestingly, membrane hyperpolarization was proposed to be negatively correlated with ribosome activity (Bosdriesz et al. 2015, Lee et al. 2019). In our experimental setup, kanamycin was administrated upon the early readaptation to the sudden osmotic downshift, during which the cells displayed an extended period of hyperpolarization (~4 hours; Fig. 3C), and thus impaired ribosome activity. Knowing that ribosomes are the primary target for aminoglycosides, we suggest that the extended period of membrane hyperpolarization averts the bactericidal activity of kanamycin in nondividing but metabolically active cells.

Bacillus subtilis enters the VBNC state and avoids antibiotic-mediated cell death

The single-cell analysis of *B. subtilis* revealed that, following salt pretreatment, a considerable fraction of the population is locked down in a metabolically active, nongrowing state. Since the removal of the antibiotic from the microfluidics chamber did not resume cell growth, we hypothesized that cells entered a deep dormant-like state associated with VBNC cells. To test our hypothesis, we cultured preadapted sporulation-deficient *B. subtilis* cells in media with antibiotics for 18 hours and estimated the number

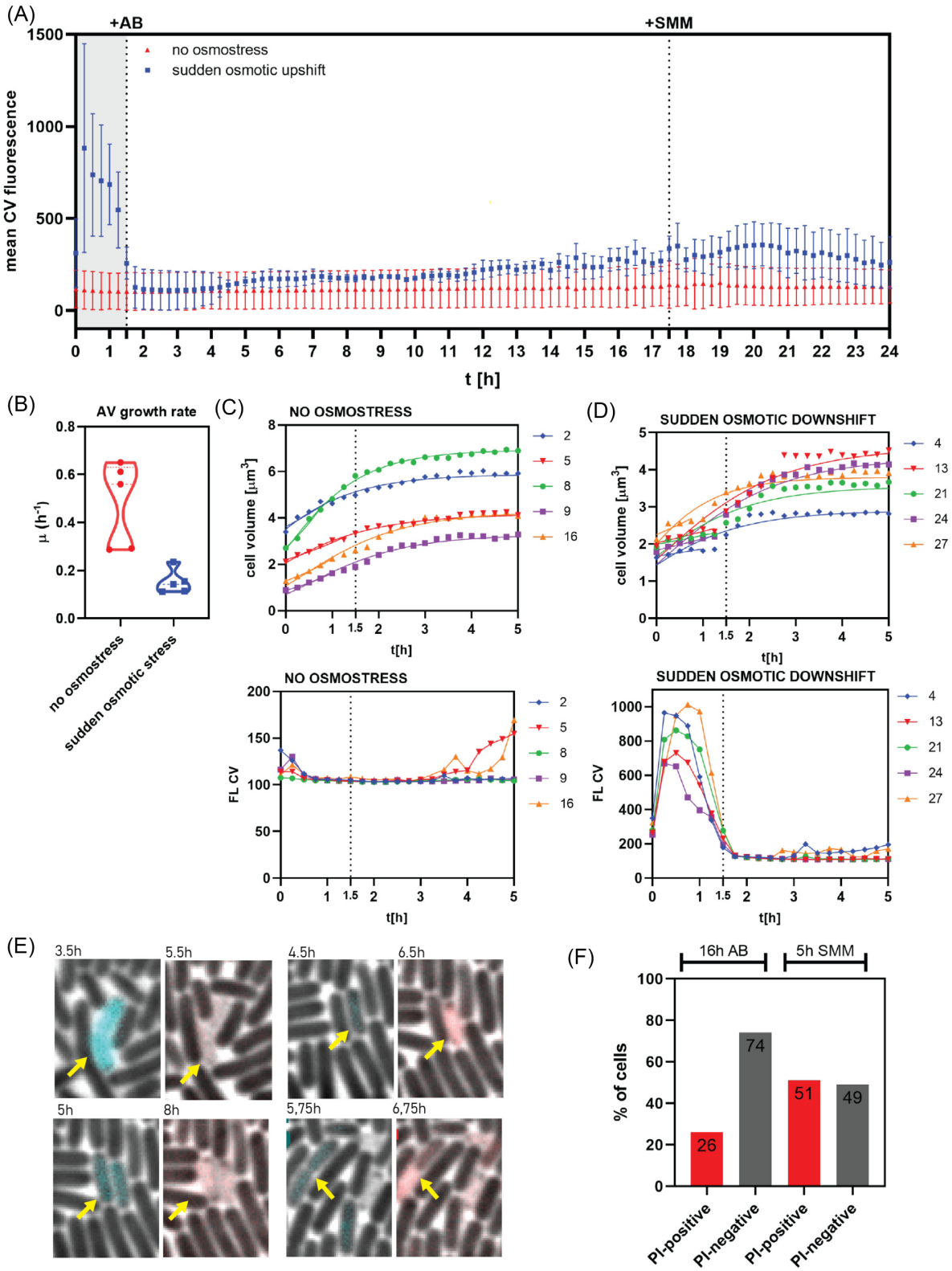

Figure 7. Single-cell analysis of metabolic activity, growth rates, and cell fate of differently preadapted *B. subtilis* 168. **(A)** Measurements of mean CV fluorescence are shown for two differently preadapted cultures: without osmostress pretreatment (the red dots) and with 0.6 M NaCl for 90 minutes (the blue dots) during 16 hours of kanamycin exposure (62.5 μg/ml) and 5 hours postantibiotic treatment. The shaded area in grey indicates the first 90 minutes of preadaptation to osmotic upshift. The dotted lines indicate the media change inside the microfluidic chambers. The error bars show the standard deviation of the CV signal. **(B)** Average growth rates (h^{-1}) of differently preadapted cells ($n = 5$ per condition). **(C)** and **(D)** Upper panels show changes in cell volume in time, indicating the cell growth of single cells ($n = 5$), whereas lower panels show corresponding mean CV fluorescence of each cell ($n = 5$). The legend on the right side of the graph shows the identifiers of single cells followed by time-lapse microscopy. **(E)** Micrographs of antibiotic-sensitive cells (no osmostress pretreatment) showing high CV fluorescent signal and subsequent increase in PI fluorescence, indicating cell death. **(F)** Estimation of damaged cells for preadapted cells after 16 hours of antibiotic exposure and 5 hours after antibiotic removal.

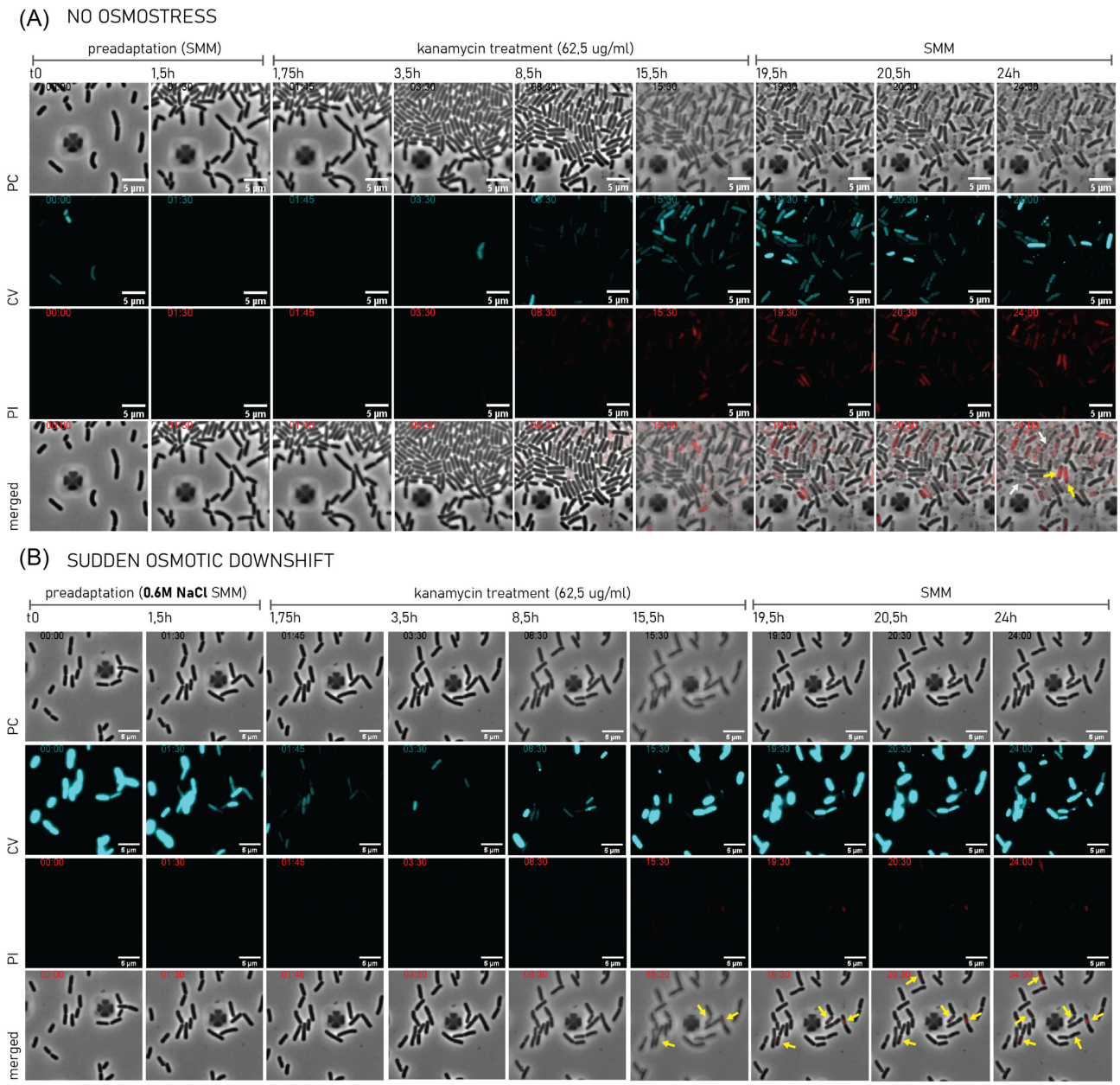

Figure 8. Metabolic activity sensing of differently pretreated cultures of *B. subtilis* 168 during and postantibiotic treatment. Micrographs **(A)** and **(B)** and show metabolic sensing to three stages of the experiment: (1) 90 minutes of preadaptation conditions without or with 0.6 M NaCl, respectively; (2) 16 hours of 62.5 μg/ml kanamycin exposure in SMM; and (3) 8 hours growth in salt- and kanamycin-free media. The upper panel of all sections shows phase-contrast images. The CV panel indicates the CV fluorescent signal of the individual cells, whereas the PI panel indicates the fluorescent signal from damaged cells. The last panel shows merged phase contrast and PI channel. The yellow arrows indicate damaged cells, whereas the white ones show lysed cells. Scale bar—5 μm.

of viable cells in the tested cultures with double staining with PI and SYTO 9 and flow cytometry. Additionally, we measured the ATP levels of the pretreated populations and determined their CFU counts on LB agar plates.

The viability assay showed that pretreatment with osmotic stress prior to antibiotic exposure significantly decreased the amount of dead cells after 18 hours of kanamycin treatment (Fig. 10). The fraction of damaged cells in the pretreated culture reached 55%, showing that approximately 45% of the population was alive (Figs 10D and 11A). However, the CFU count data revealed that only a small fraction of cells identified as alive could grow on LB agar plates (~0.0007%) compared to the control grown without kanamycin (Fig. 11B). Additionally, the analysis of intracellular ATP levels after 18 hours of the antibiotic treatment showed that the preadapted population displays a similar level of ATP to the nonstressed, culturable cells (Fig. 11C).

Discussion

In this study, we elucidated *B. subtilis*' adaptation to osmotic environmental stress and its effect on antibiotic tolerance. Combining population-wide and single-cell analysis, we demonstrated that *B. subtilis* exposed to osmotic upshift modulates its metabolic activity and becomes resistant to the aminoglycoside group of antibiotics. The first indication of the reduced metabolic activity was a significantly reduced growth rate (~2,5-fold) of osmostressed

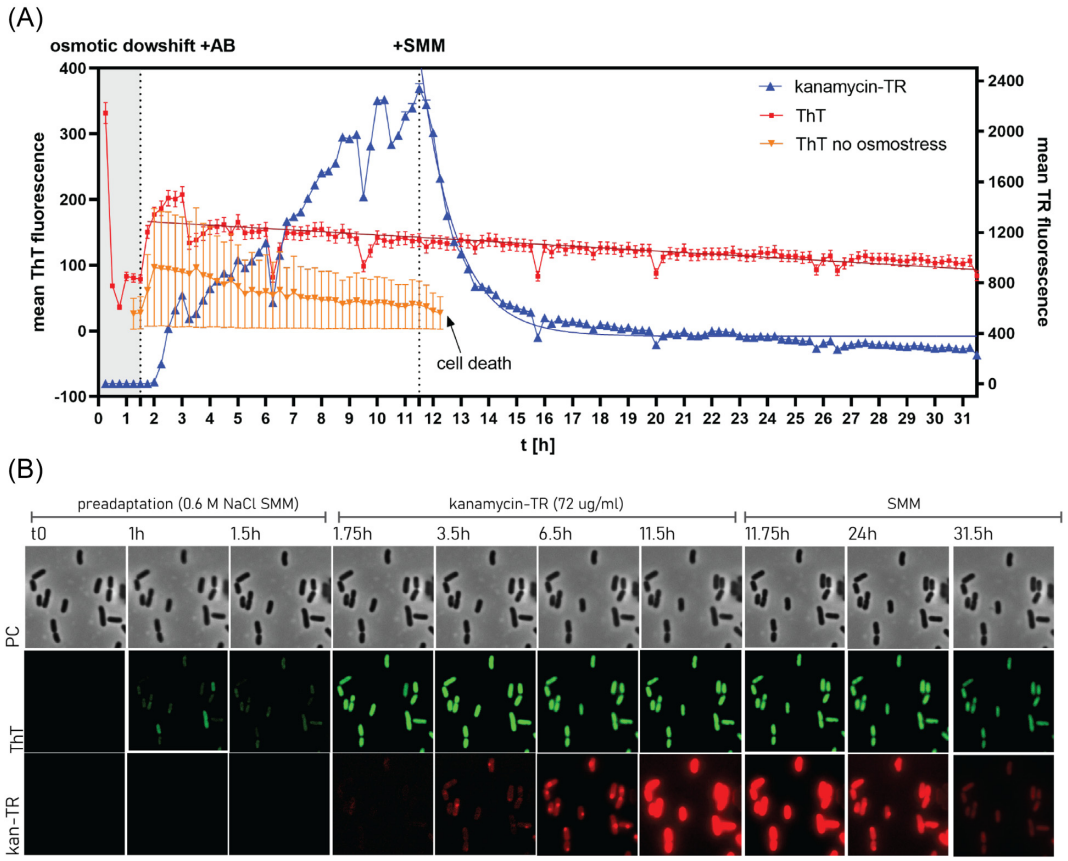

Figure 9. Osmotic downshift and synchronal kanamycin exposure cause long-lasting membrane hyperpolarization. **(A)** Measurements of mean ThT (the red dots, left y-axis) and kanamycin-Texas Red (the blue dots, right y-axis) fluorescence are shown for preadapted cells. Additionally, the orange dots (left y-axis) show the mean ThT signal from kanamycin-sensitive cells (no osmostress). The grey shaded area indicates the first 90 minutes of preadaptation to osmotic upshift. The dotted lines indicate the media change. **(B)** Micrographs of preadapted cells were challenged with sudden osmotic downshift and kanamycin-Texas Red exposure (72 μg/ml) and subsequently washed with SMM. The upper panel shows phase-contrast images. The ThT panel indicates the individual cells' ThT fluorescent signal (membrane potential), whereas the kan-TR panel indicates the fluorescent signal from accumulated kanamycin-Texas Red.

cultures compared to the control without the pretreatment step (Fig. 2). The second evidence was demonstrated with membrane potential measurements, indicating diminished membrane potential of osmotically stressed cells, confirming reduced respiration and metabolic rates (Fig. 3).

Osmostress pretreatment promotes aminoglycoside tolerance in *B. subtilis*

We observed and characterized two antibiotic-tolerant phenotypes depending on the osmotic upshift and time of kanamycin administration. The first one, in which cells exposed to sustained osmotic upshift became antibiotic insensitive while maintaining active growth, and the second one, where the adaptation to the osmotic upshift and subsequent antibiotic stress with no osmotic stress gave rise to a nondividing population (Fig. 2). It could be speculated that in both cases, the observed phenotypes are mainly a direct result of the decreased membrane potential of the osmostressed cells (Fig. 3), which has previously been proposed to impair the antibiotic uptake across the membrane (Ramirez and Tolmasky 2010, Damper and Epstein 1981, Taber et al. 1987). However, recent work by Bruni and Kralj (2020) has shown that membrane voltage is not essential for aminoglycosides uptake but is required for bactericidal activity. Increased tolerance to aminoglycoside-induced cell damage was also reflected by reduced accumulation of ROS in the case of sudden osmotic downshift and sustained osmotic upshift (Fig. 4). Our data showed that cells experiencing sudden osmotic downshift and sustained osmotic upshift significantly reduce ROS levels when exposed to lethal concentrations of kanamycin compared to untreated cells.

Uptake of aminoglycosides in the presence of sodium chloride is limited due to weaker electrostatic binding of kanamycin to the cell envelope

Using time-lapse microscopy and a microfluidics system, our study adds new insight into the uptake of aminoglycosides under osmotic stress at the single-cell level. We provide evidence for the increased tolerance towards kanamycin under sustained osmotic upshift caused by limited drug accumulation inside the cytoplasm. We suggest that this effect is primarily due to the kanamycin-cell surface interactions in a high ionic strength environment and second due to disturbances in the membrane potential and reduced growth rates of treated cells. These findings are consistent with earlier work in *Escherichia coli* from Plotz et al. (1961), which revealed that a wash with salt media could remove cell-bound streptomycin. Similarly, Taber and Halfenger (1976) confirmed that ionic interaction between sodium chloride and kanamycin are crucial for the initial antibiotic binding in *B. subtilis*.

Moreover, in the case of sustained osmotic stress and kanamycin exposure, the 90 minutes of 0.6 M NaCl pretreatment

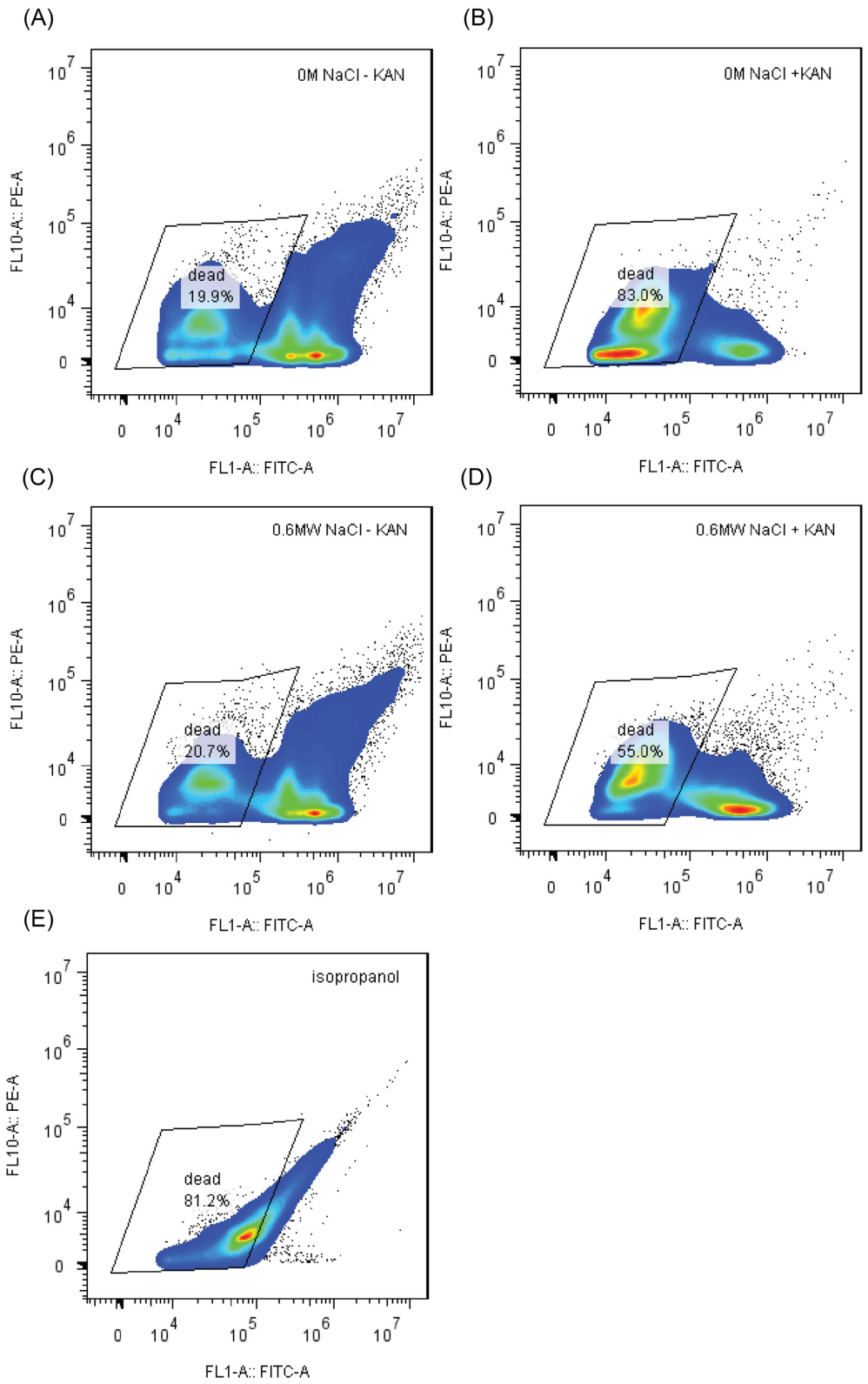

Figure 10. Estimated fractions of dead cells in kanamycin-treated cultures of *B. subtilis* 168 Δ*sigF*. A viability assay was performed for different preadapted cultures exposed to a lethal kanamycin concentration (62.5 μg/ml) for 18 hours. **(A)** Control conditions without osmotic stress pretreatment and kanamycin, **(B)** cells without osmotic stress pretreatment with kanamycin, **(C)** cells pretreated for 90 minutes with 0.6 M NaCl without antibiotic stress, and **(D)** cells pretreated for 90 minutes with 0.6 M NaCl, exposed to antibiotic stress. The *x*-axis represents the SYTO-9 fluorescent signal, whereas the *y*-axis PI fluorescent signal. The total sample size was 100 000 individuals.

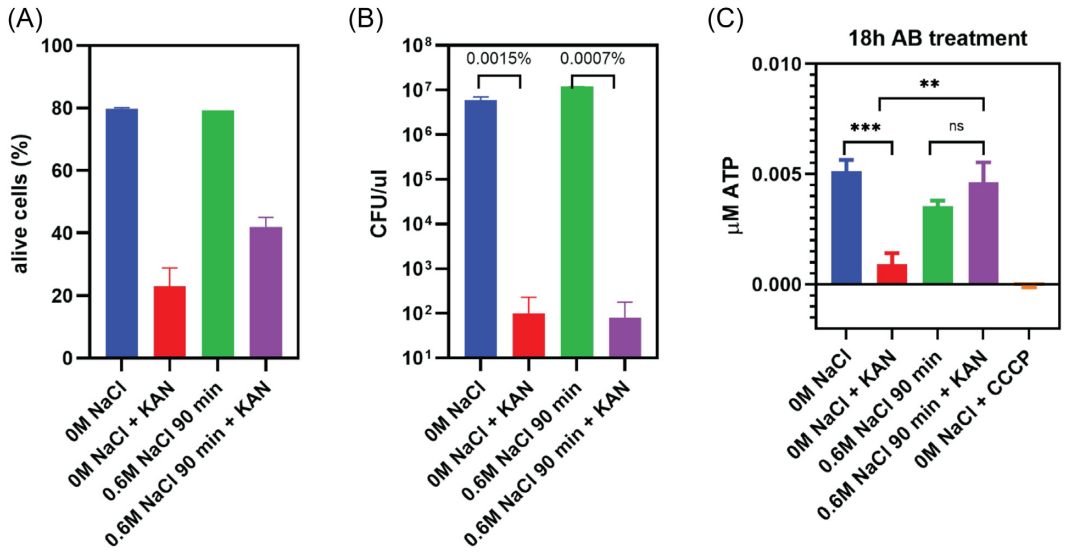

Figure 11. Culturability on LB media and intercellular ATP levels of *B. subtilis* 168 Δ*sigF* after 18 hours of antibiotic treatment. (A) Estimation of alive cells concentration based on PI staining and flow cytometry data. Error bars (SEM, $n = 2$), sample size 100 000 events. (B) Resuscitation of nongrowing cells on LB agar plates represented by CFUs/μl. Error bars (SEM, $n = 2$). The percentages show the fraction of the population resistant to kanamycin and able to regrow. (C) Intracellular ATP measurements of differently preadapted cultures with or without 18 hours of kanamycin exposure (showed as ATP μM/OD600). Error bars (SEM, $n = 3$) *t*-test: ** $P = 0.0036$; *** $P = 0.0005$; and ns—not significant.

period was not essential for the protective effect to occur (Fig. 2D). We propose that the presence of a high concentration of sodium near the cell's surface outcompetes the electrostatic binding of kanamycin and hence, limits the drug's intake. This could explain the increase in fluorescent signal from kanamycin-Texas Red when the osmotically stressed cells were washed with salt-free media (Fig. 6H and I). Furthermore, continuous growth in SMM with 0.6 M glycerol (imposing nonionic stress) did not protect the cells from kanamycin (Figure S3, Supporting Information), being strong evidence of the importance of the ionic strength of media in kanamycin efficacy.

Bacillus subtilis cells are locked into a nondividing but metabolically active state and become kanamycin-tolerant

Our study showed for the first time that the shifts in the environment's osmolarity and simultaneous kanamycin treatment promote cells to enter a nondividing but metabolically active state. With time-lapse microscopy and kanamycin-Texas Red conjugate, we demonstrated that cells entrapped in a nondividing state could efficiently accumulate kanamycin, similarly to the untreated cells (Fig. 6G). We showed that these nondividing cells are metabolically active and can withstand long hours of antibiotic exposure (Figs 7 and 8).

Furthermore, consistently to previous studies, kanamycin-tolerant cells were found to display prolonged membrane hyperpolarization (Fig. 9), caused by the adaptation to sudden osmotic downshift (Misra et al. 2013, Rojas and Huang 2018) and simultaneous kanamycin treatment (Lobritz et al. 2015, Lee et al. 2019, Bruni and Kralj 2020). Because membrane hyperpolarization is inversely correlated with ribosomal activity (Bosdriesz et al. 2015, Lee et al. 2019), we believe that prolonged membrane hyperpolarization protects *B. subtilis* cells from the bactericidal effects of kanamycin—a ribosome-targeting antibiotic. In line with our hypothesis, we demonstrated that 3 hours of readaptation to the neutral osmolarity prior to antibiotic treatment resensitized *B. subtilis* to kanamycin (Fig. 6D), suggesting that cells that reached electrical homeostasis, increased ribosomal activity, and entered a new steady-state, are more sensitive to kanamycin.

Previous studies by Fridman et al. (2014) demonstrated that antibiotic-tolerant *E. coli* displayed a long lag time before the regrowth in antibiotic-free media, and its duration was directly correlated with the period of the antibiotic exposure. In our current work, we observed that pretreated *B. subtilis* cells could not resume division even after 20 hours post-antibiotic treatment in permissible growth conditions, a double of the duration of the antibiotic treatment (Fig. 9). However, after this period, cells still displayed a moderate fluorescent signal from kanamycin-Texas Red and relatively high membrane hyperpolarization, suggesting that the reminiscent amount of the antibiotic could extend the regrowth lag time (Fig. 9B). Nevertheless, the gradual decay of the ThT and kanamycin–Texas Red fluorescent signals may indicate that the cells are still able to resume division after the antibiotic is completely removed.

A subpopulation of nondividing but metabolically active cells enters the VBNC state

Finally, we showed that part of the population of nondividing but metabolically active cells entered the VBNC state. With flow cytometry, we estimated the amount of alive cells in the liquid culture of preadapted cells after 18 hours of kanamycin treatment (Fig. 10D). However, only a small fraction of these cells could form colonies on LB agar plates (Fig. 11B).

The VBNC state has been observed in many bacteria and proposed as a survival mechanism allowing cells to withstand long exposure to many adverse conditions (Oliver 2010, Li et al. 2014). Despite their detectable metabolic activity, VBNC cells lost their ability to form colonies on a routine media (Pinto et al. 2015). However, they can be resuscitated with appropriate environmental stimuli or permissive growth conditions (Oliver 2010, Li et al. 2014). In *Vibrio vulnificus*, it has been observed that VBNC cells, induced under the cold shock treatment, displayed increased catalase activity upon resuscitation (Kong et al. 2004). In this case, a catalase-negative mutant, incapable of hydrogen peroxide detoxi-

fication, became nonculturable at ambient temperature, suggesting that H_2O_2-induced stress promotes entry into the VBNC state. Moreover, when VBNC cells were plated onto standard media supplemented with ROS mitigating agents like catalase or sodium pyruvate, the fraction of culturable cells increased significantly. Similar observations were made for other microorganisms (Wai et al. 2000, Masmoudi et al. 2010, Senoh et al. 2015, Hamabata et al. 2021), showing that resuscitation of VBNC cells likely depends on their ability to neutralize highly ROS generated upon stress conditions. Notably, a recent study by Hong et al. (2019) demonstrated that *E. coli* cells displayed a self-amplifying accumulation of toxic ROS postantibiotic treatment, which directly contributed to cell death. Surprisingly, this effect was averted with catalase supplementation to the LB agar (Hong et al. 2019), similarly to what was observed in the VBNC cells resuscitation studies. In the current study, pretreated *B. subtilis* cells showed reduced ROS accumulation compared to the kanamycin-sensitive cells. We suggest that reduced ROS levels might not contribute to cell death but instead drive cells into a low metabolic state to avoid the secondary lethal damage, however, further studies are needed to confirm this hypothesis.

ATP depletion and aggresome formation in *B. subtilis* VBNC cells

Recently it has been proposed that bacteria enter the VBNC state due to increased protein aggregation caused by gradual cellular ATP depletion (Pu et al. 2019). Conversely, our study did not show the protein aggregation phenotype upon antibiotic treatment in the pretreated cells. We suggest that the physiological changes induced under the osmotic upshift, including elevated pools of osmoprotectants (in our experimental setup, only proline), might prevent excessive protein aggregation during antibiotic stress. Intriguingly, except for its osmoprotective properties, proline has been shown to act as a chemical protein chaperon that can stabilize protein structures and inhibit aggregation during protein refolding (Auton and Bolen 2005, Samuel et al. 2000).

In regards to intracellular ATP levels, our data showed that after 18 hours of continuous antibiotic treatment, the VBNC cells displayed similar levels of ATP as culturable cells, being in agreement with other studies showing ATP levels in VBNC cells to be similar or higher than culturable cells (Beumer et al. 1992, Su et al. 2015, Zhao et al. 2016). These similar levels of intracellular ATP pools in VBNC and culturable cells would contradict the dormancy continuum theory proposed by Pu et al. (2019). It seems that despite the similarities in the formation of persister and VBNC cells, the entry into the deeper dormant state for pretreated *B. subtilis* cells does not depend on ATP depletion.

Conclusions

We demonstrated that *B. subtilis* population enters the VBNC state due to the metabolic and biochemical changes prior to antibiotic treatment, including reduced metabolic activity and prolonged membrane hyperpolarization. Importantly, we show that besides spore formation (Errington 2003) and switching to oligotrophic growth due to nutrient depletion (Gray et al. 2019), *B. subtilis* populations can persist in a VBNC state and become tolerant to kanamycin. Although *B. subtilis* is not a human pathogen, our work can be of high relevance for studying the formation of the VBNC cells in pathogenic Gram-positive bacteria experiencing frequent environmental changes, including human pathogens.

Acknowledgements

We thank Prof. Erhard Bremer and Dr. Tamara Hoffmann for helpful discussions on osmostress in Bacillus subtilis.

Supplementary data

Supplementary data are available at *FEMSML* online.

Conflicts of interest statement. None declared.

References

Allison KR, Brynildsen MP, Collins JJ. Metabolite-enabled eradication of bacterial persisters by aminoglycosides. *Nature* 2011;**473**:216–20.

Amato SM, Orman MA, Brynildsen MP. Metabolic control of persister formation in *Escherichia coli*. *Mol Cell* 2013;**50**:475–87.

Anand A, Chen K, Yang L. *et al.* Adaptive evolution reveals a tradeoff between growth rate and oxidative stress during naphthoquinone-based aerobic respiration. *Proc Natl Acad Sci* 2019;**116**:25287–92.

Auton M, Bolen DW. Predicting the energetics of osmolyte-induced protein folding/unfolding. *Proc Natl Acad Sci* 2005;**102**:15065–8. https://doi.org/10.1073/pnas.0507053102.

Ayrapetyan M, Williams T, Oliver JD. Relationship between the viable but non-culturable state and antibiotic persister cells. *J Bacteriol* 2018;**200**:e00249–18.

Ayrapetyan M, Williams TC, Baxter R. *et al.* Viable but nonculturable and persister cells coexist stochastically and are induced by human serum. *Infect Immun* 2015a;**83**:4194–203.

Ayrapetyan M, Williams TC, Oliver JD. Bridging the gap between viable but non-culturable and antibiotic persistent bacteria. *Trends Microbiol* 2015b;**23**:7–13.

Balaban NQ, Merrin J, Chait R. *et al.* Bacterial persistence as a phenotypic switch. *Science* 2004;**305**:1622–5.

Beumer RR, de Vries J, Rombouts FM. *Campylobacter jejuni* nonculturable coccoid cells. *Int J Food Microbiol* 1992;**15**:153–63.

Borovinskaya MA, Pai RD, Zhang W *et al.* Structural basis for aminoglycoside inhibition of bacterial ribosome recycling. *Nat Struct Mol Biol* 2007;**14**:727–32.

Bosdriesz E, Molenaar D, Teusink B *et al.* How fast-growing bacteria robustly tune their ribosome concentration to approximate growth-rate maximization. *FEBS J* 2015;**282**:2029–44.

Bremer E, Krämer R. Responses of microorganisms to osmotic stress. *Annu Rev Microbiol* 2019;**73**:313–34.

Brill J, Hoffmann T, Bleisteiner M. *et al.* Osmotically controlled synthesis of the compatible solute proline is critical for cellular defense of *Bacillus subtilis* against high osmolarity. *J Bacteriol* 2011;**193**:5335–46.

Bruni GN, Kralj JM. Membrane voltage dysregulation driven by metabolic dysfunction underlies bactericidal activity of aminoglycosides. *ELife* 2020;**9**:e58706.

Busse HJ, Wöstmann C, Bakker EP. The bactericidal action of streptomycin: membrane permeabilization caused by the insertion of mistranslated proteins into the cytoplasmic membrane of *Escherichia coli* and subsequent caging of the antibiotic inside the cells due to degradation of these proteins. *J Gen Microbiol* 1992;**138**:551–61.

Damper PD, Epstein W. Role of the membrane potential in bacterial resistance to aminoglycoside antibiotics. *Antimicrob Agents Chemother* 1981;**20**:803–8.

Davis BD, Chen LL, Tai PC. Misread protein creates membrane channels: an essential step in the bactericidal action of aminoglycosides. *Proc Natl Acad Sci* 1986;**83**:6164–8.

Ducret A, Quardokus EM, Brun YV. MicrobeJ, a tool for high throughput bacterial cell detection and quantitative analysis. *Nat Microbiol* 2016;**1**:1–7.

Earl AM, Losick R, Kolter R. Ecology and genomics of *Bacillus subtilis*. *Trends Microbiol* 2008;**16**:269.

Errington J. Regulation of endospore formation in *Bacillus subtilis*. *Nat Rev Microbiol* 2003;**1**:117–26.

Ezraty B, Vergnes A, Banzhaf M. *et al.* Fe-S cluster biosynthesis controls uptake of aminoglycosides in a ROS-less death pathway. *Science* 2013;**340**:1583–7.

Fauvart M, De Groote VN, Michiels J. Role of persister cells in chronic infections: clinical relevance and perspectives on anti-persister therapies. *J Med Microbiol* 2011;**60**:699–709.

Fisher RA, Gollan B, Helaine S. Persistent bacterial infections and persister cells. *Nat Rev Microbiol* 2017;**15**:453–64.

Fridman O, Goldberg A, Ronin I. *et al.* Optimization of lag time underlies antibiotic tolerance in evolved bacterial populations. *Nature* 2014;**513**:418–21.

Godard T, Zühlke D, Richter G. *et al.* Metabolic rearrangements causing elevated proline and polyhydroxybutyrate accumulation during the osmotic adaptation response of *Bacillus megaterium*. *Front Bioeng Biotechnol* 2020;**8**:47.

Gray DA, Dugar G, Gamba P. *et al.* Extreme slow growth as alternative strategy to survive deep starvation in bacteria. *Nat Commun* 2019;**10**:890.

Guo MS, Gross CA. Stress induced remodeling of the bacterial proteome. *Curr Biol* 2014;**24**:R424–34.

Hahne H, Mäder U, Otto A *et al.* A comprehensive proteomics and transcriptomics analysis of *Bacillus subtilis* salt stress adaptation. *J Bacteriol* 2010;**192**:870–82.

Hamabata T, Senoh M, Iwaki M. *et al.* Induction and resuscitation of viable but nonculturable *Corynebacterium diphtheriae*. *Microorganisms* 2021;**9**:927.

Hancock RE, Raffle VJ, Nicas TI. Involvement of the outer membrane in gentamicin and streptomycin uptake and killing in *Pseudomonas aeruginosa*. *Antimicrob Agents Chemother* 1981;**19**:777–85.

Harwood CR, Cutting SM. *Molecular Biological Methods for Bacillus*. Hoboken: Wiley, 1990.

Helaine S, Kugelberg E. Bacterial persisters: formation, eradication, and experimental systems. *Trends Microbiol* 2014;**22**:417–24.

Hendon-Dunn CL, Doris KS, Thomas SR. *et al.* A flow cytometry method for rapidly assessing *Mycobacterium tuberculosis* responses to antibiotics with different modes of action. *Antimicrob Agents Chemother* 2016;**60**:3869–83.

Hoffmann T, Bremer E. Management of osmotic stress by *Bacillus subtilis*: genetics and physiology. In: *Stress and Environmental Regulation of Gene Expression and Adaptation in Bacteria*. Hoboken: John Wiley & Sons, Ltd, 2016, 657–76. DOI: 10.1002/9781119004813.ch63.

Hong Y, Zeng J, Wang X *et al.* Post-stress bacterial cell death mediated by reactive oxygen species. *Proc Natl Acad Sci* 2019;**116**:10064–71.

Humphries J, Xiong L, Liu J. *et al.* Species-independent attraction to biofilms through electrical signaling. *Cell* 2017;**168**:200–9.

Kadurugamuwa JL, Clarke AJ, Beveridge TJ. Surface action of gentamicin on *Pseudomonas aeruginosa*. *J Bacteriol* 1993a;**175**:5798–805.

Kadurugamuwa JL, Lam JS, Beveridge TJ. Interaction of gentamicin with the A band and B band lipopolysaccharides of *Pseudomonas aeruginosa* and its possible lethal effect. *Antimicrob Agents Chemother* 1993b;**37**:715–21.

Keren I, Wu Y, Inocencio J. *et al.* Killing by bactericidal antibiotics does not depend on reactive oxygen species. *Science* 2013;**339**:1213–6.

Kohanski MA, Dwyer DJ, Collins JJ. How antibiotics kill bacteria: from targets to networks. *Nat Rev Microbiol* 2010;**8**:423–35.

Kohanski MA, Dwyer DJ, Hayete B. *et al.* A common mechanism of cellular death induced by bactericidal antibiotics. *Cell* 2007;**130**:797–810.

Kohanski MA, Dwyer DJ, Wierzbowski J. *et al.* Mistranslation of membrane proteins and two-component system activation trigger antibiotic-mediated cell death. *Cell* 2008;**135**:679–90.

Kohlstedt M, Sappa PK, Meyer H. *et al.* Adaptation of *Bacillus subtilis* carbon core metabolism to simultaneous nutrient limitation and osmotic challenge: a multi-omics perspective. *Environ Microbiol* 2014;**16**:1898–917.

Kong I-S, Bates TC, Hülsmann A. *et al.* Role of catalase and oxyR in the viable but nonculturable state of *Vibrio vulnificus*. *FEMS Microbiol Ecol* 2004;**50**:133–42.

Kotte O, Volkmer B, Radzikowski JL. *et al.* Phenotypic bistability in *Escherichia coli*'s central carbon metabolism. *Mol Syst Biol* 2014;**10**:736.

Krämer CEM, Singh A, Helfrich S. *et al.* Non-invasive microbial metabolic activity sensing at single cell level by perfusion of calcein acetoxymethyl ester. *PLoS ONE* 2015;**10**:e0141768.

Kubistova L, Dvoracek L, Tkadlec J. *et al.* Environmental stress affects the formation of *Staphylococcus aureus* persisters tolerant to antibiotics. *Microb Drug Resist* 2018;**24**:547–55.

Kussell E, Kishony R, Balaban NQ. *et al.* Bacterial persistence. *Genetics* 2005;**169**:1807–14.

Lee DD, Galera-Laporta L, Bialecka-Fornal M. *et al.* Magnesium flux modulates ribosomes to increase bacterial survival. *Cell* 2019;**177**:352–60.

Leviton IM, Fraimow HS, Carrasco N. *et al.* Tobramycin uptake in *Escherichia coli* membrane vesicles. *Antimicrob Agents Chemother* 1995;**39**:467–75.

Lewis K. Persister cells, dormancy and infectious disease. *Nat Rev Microbiol* 2007;**5**:48–56.

Li L, Mendis N, Trigui H. *et al.* The importance of the viable but non-culturable state in human bacterial pathogens. *Front Microbiol* 2014;**5**:258.

Lobritz MA, Belenky P, Porter CBM. *et al.* Antibiotic efficacy is linked to bacterial cellular respiration. *Proc Natl Acad Sci* 2015;**112**, 8173–80.

Manuse S, Shan Y, Canas-Duarte SJ. *et al.* Bacterial persisters are a stochastically formed subpopulation of low-energy cells. *PLoS Biol* 2021;**19**:e3001194.

Masmoudi S, Denis M, Maalej S. Inactivation of the gene katA or sodA affects the transient entry into the viable but non-culturable response of *Staphylococcus aureus* in natural seawater at low temperature. *Mar Pollut Bull* 2010;**60**:2209–14.

Misra G, Rojas ER, Gopinathan A. *et al.* Mechanical consequences of cell-wall turnover in the elongation of a Gram-positive bacterium. *Biophys J* 2013;**104**:2342–52.

Mulcahy LR, Burns JL, Lory S. *et al.* Emergence of *Pseudomonas aeruginosa* strains producing high levels of persister cells in patients with cystic fibrosis. *J Bacteriol* 2010;**192**:6191–9.

Nichols WW, Young SN. Respiration-dependent uptake of dihydrostreptomycin by *Escherichia coli*. Its irreversible nature and lack of evidence for a uniport process. *Biochem J* 1985;**228**:505–12.

Nieß A, Siemann-Herzberg M, Takors R. Protein production in *Escherichia coli* is guided by the trade-off between intracellular substrate availability and energy cost. *Microb Cell Fact* 2019;**18**:8.

Nowakowska J, Oliver JD. Resistance to environmental stresses by *Vibrio vulnificus* in the viable but non-culturable state. *FEMS Microbiol Ecol* 2013;**84**:213–22.

O'Brien EJ, Utrilla J, Palsson BO. Quantification and classification of *E. coli* proteome utilization and unused protein costs across environments. *PLoS Comput Biol* 2016;**12**:e1004998.

Oliver JD (2000). The public health significance of viable but non-culturable bacteria. In: Colwell RR., Grimes DJ. (eds). *Non-Culturable Microorganisms in the Environment*. Berlin: Springer. 277–300.

Oliver JD, Bockian R. In vivo resuscitation, and virulence towards mice, of viable but non-culturable cells of *Vibrio vulnificus*. *Appl Environ Microbiol* 1995;**61**:2620–3.

Oliver JD, Dagher M, Linden K. Induction of *Escherichia coli* and *Salmonella typhimurium* into the viable but non-culturable state following chlorination of wastewater. *J Water Health* 2005;**3**: 249–57.

Oliver JD. Recent findings on the viable but non-culturable state in pathogenic bacteria. *FEMS Microbiol Rev* 2010;**34**:415–25.

Pinto D, Santos MA, Chambel L. Thirty years of viable but non-culturable state research: unsolved molecular mechanisms. *Crit Rev Microbiol* 2015;**41**:61–76.

Plotz PH, Dubin DT, Davis BD. Influence of salts on the uptake of streptomycin by *Escherichia coli*. *Nature* 1961;**191**:1324–5.

Prindle A, Liu J, Asally M. *et al.* Ion channels enable electrical communication in bacterial communities. *Nature* 2015;**527**: 59–63.

Pu Y, Li Y, Jin X. *et al.* ATP-dependent dynamic protein aggregation regulates bacterial dormancy depth critical for antibiotic tolerance. *Mol Cell* 2019;**73**:143–56.

Radzikowski JL, Vedelaar S, Siegel D. *et al.* Bacterial persistence is an active σS stress response to metabolic flux limitation. *Mol Syst Biol* 2016;**12**:882.

Ramirez MS, Tolmasky ME. Aminoglycoside modifying enzymes. *Drug Resist Updat* 2010;**13**:151–71.

Ray JCJ, Wickersheim ML, Jalihal AP. *et al.* Cellular growth arrest and persistence from enzyme saturation. *PLoS Comput Biol* 2016;**12**:e1004825.

Rittershaus ESC, Baek S, Sassetti CM. The normalcy of dormancy. *Cell Host Microbe* 2013;**13**:643–51.

Rojas ER, Huang KC, Theriot JA. Homeostatic cell growth is accomplished mechanically through membrane tension inhibition of cell-wall synthesis. *Cell Syst* 2017;**5**:578–90.

Rojas ER, Huang KC. Regulation of microbial growth by turgor pressure. *Curr Opin Microbiol* 2018;**42**:62–70.

Samuel D, Kumar TK, Ganesh G *et al.* Proline inhibits aggregation during protein refolding. *Protein Sci: A Publication of the Protein Society* 2000;**9**:344–52.

Schroeter R, Hoffmann T, Voigt B. *et al.* Stress responses of the industrial workhorse *Bacillus licheniformis* to osmotic challenges. *PLoS ONE* 2013;**8**:e80956.

Senoh M, Hamabata T, Takeda Y. A factor converting viable but non-culturable *Vibrio cholerae* to a culturable state in eukaryotic cells is a human catalase. *MicrobiologyOpen* 2015;**4**:589–96.

Sévin DC, Sauer U. Ubiquinone accumulation improves osmotic-stress tolerance in *Escherichia coli*. *Nat Chem Biol* 2014;**10**:266–72.

Sévin DC, Stählin JN, Pollak GR. *et al.* Global metabolic responses to salt stress in fifteen species. *PLoS ONE* 2016;**11**:e0148888.

Soufi B, Krug K, Harst A. *et al.* Characterization of the *E. coli* proteome and its modifications during growth and ethanol stress. *Front Microbiol* 2015;**6**:103.

Su X, Sun F, Wang Y. *et al.* Identification, characterization and molecular analysis of the viable but non-culturable *Rhodococcus biphenylivorans*. *Sci Rep* 2015;**5**:18590.

Taber H, Halfenger GM. Multiple-aminoglycoside-resistant mutants of *Bacillus subtilis* deficient in accumulation of kanamycin. *Antimicrob Agents Chemother* 1976;**9**:251–9.

Taber HW, Mueller JP, Miller PF. *et al.* Bacterial uptake of aminoglycoside antibiotics. *Microbiol Rev* 1987;**51**:439–57.

Wai SN, Mizunoe Y, Takade A. *et al.* A comparison of solid and liquid media for resuscitation of starvation- and low-temperature-induced non-culturable cells of *Aeromonas hydrophila*. *Arch Microbiol* 2000;**173**:307–10.

Whatmore AM, Chudek JA, Reed RH. The effects of osmotic upshock on the intracellular solute pools of *Bacillus subtilis*. *J Gen Microbiol* 1990;**136**:2527–35.

Wood JM. Bacterial osmoregulation: a paradigm for the study of cellular homeostasis. *Annu Rev Microbiol* 2011;**65**:215–38.

Zeder M, Kohler E, Zeder L *et al.* A novel algorithm for the determination of bacterial cell volumes that is unbiased by cell morphology. *Microsc Microanal* 2011;**17**:799–809.

Zhao F, Wang Y, An H *et al.* New insights into the formation of viable but nonculturable *Escherichia coli* O157:H7 induced by high-pressure CO2. *MBio* 2016;**7**:e00961–16.